OBSERVATIONAL CHALLENGES IN ASSESSING THE AEROSOL INDIRECT AND SEMI-DIRECT EFFECT

by

Erik M. Gould

A thesis submitted in partial fulfillment of

the requirements for the degree of

Master of Science

(Atmospheric and Oceanic Science)

at the

UNIVERSITY OF WISCONSIN-MADISON

2014

Declaration of Authorship

I, Erik M. Gould, declare that this thesis titled, 'Observational Challenges in Assessing the Aerosol Indirect and Semi-Direct Effect' and the work presented in it are my own.

Erik M. Gould _____
Author

_____
Signature

I hereby approve and recommend for acceptance this work in partial fulfillment of the requirements for the degree of Master of Science:

Ralf Bennartz _____
Faculty Member

_____
Signature

Tristan S. L'Ecuyer _____
Faculty Member

_____
Signature

Grant W. Petty _____
Faculty Member

_____
Signature

Abstract

This study aims to identify the challenges associated with assessing the aerosol indirect and semi-direct effect from space-borne instruments as well as identify some robust aerosol signatures. This study utilizes geographically and temporally colocated data sets of aerosol, cloud, and precipitation properties obtained from the MODerate resolution Imaging Spectroradiometer (MODIS) instrument aboard the Aqua satellite, the Cloud-Aerosol LIdar with Orthogonal Polarization instrument aboard the Cloud-Aerosol Lidar and Infrared Pathfinder Satellite Observations satellite, and the Cloud Profiling Radar aboard the CloudSat satellite. The focus of the study is on a region of the southeastern Atlantic Ocean off the coast of Namibia. This region is characterized by a strong and intense seasonal biomass burning cycle. The seasonality of the biomass burning events allows for the analysis of air masses with a large distribution of aerosol concentrations. Statistical analysis included looking at correlations between ten different aerosol metrics as well as correlations between these metrics and a variety of cloud macro- and micro-physical parameters (e.g. cloud droplet number concentration and effective radius). This study found a correlation between MODIS Aerosol Index, MODIS Aerosol Optical Depth, CALIOP clear sky integrated elevated aerosol boundary layer backscatter, and CALIOP integrated elevated aerosol boundary layer backscatter. In agreement with previous work, an increase in aerosol concentration is correlated with an increase in cloud droplet number concentration and a decrease in effective radius. Additionally, an increase in aerosols touching the cloud is correlated with a decrease in the probability of precipitation and an increase in aerosols above the cloud is correlated with an increase in the probability of precipitation.

Acknowledgements

I would like to acknowledge my advisers, Drs. Ralf Bennartz and Tristan L'Ecuyer, for their guidance while I completed this thesis. I would also like to thank the NASA Langley Research Center Atmospheric Science Data Center for the CALIPSO data, the Cooperative Institute for Research in the Atmosphere (CIRA) for the CloudSat data, and the Goddard Earth Sciences Data and Information Services Center (GES-DISC) for the MODIS data.

Contents

List of Figures

List of Tables

Chapter 1

Introduction

Aerosols play an important role in the radiation and energy budget of Earth as well as in the hydrologic cycle. Aerosols affect the radiation and energy budget through the direct aerosol effect, the semi-direct aerosol effect, and two indirect aerosol effects. The direct aerosol effect is due to the absorptive and scattering properties of aerosols themselves. Most aerosols are efficient at scattering incoming shortwave solar radiation; this leads to an increase in the amount of radiation reflected back to space in a column with a heavy aerosol load. Increasing the amount of incoming solar radiation that is reflected back to space has a negative (cooling) effect on the climate. The semi-direct aerosol effect occurs when absorbing aerosols warm an atmospheric layer and either hinder cloud formation or cause cloud droplets to evaporate (Ackerman et al. 2000). This might also lead to the suppression of

precipitation in the affected region. Until recently, this effect was believed to have a net warming effect on the planet. However, there is now evidence that the semi-direct effect may have a net cooling effect on the climate (Kaufman et al. 2005; Penner et al. 2003).

As described in the Intergovernmental Panel on Climate Change Fourth Assessment Report (IPCC-4AR), the indirect aerosol effect can be further divided into the first and second indirect effects (Forster and Ramaswamy 2007). The first indirect effect, originally proposed by Twomey (1974), is a theory that describes aerosol effects on radiative forcing due to aerosols altering microphysical cloud properties. The presence of aerosols in a cloud layer increases the number of cloud condensation nuclei (CCN). An increase in CCN leads to a greater number of cloud droplets within a cloud, which will then increase the optical depth of the cloud since an incoming photon will encounter and be scattered by more particles. This, in turn, leads to an increase in the albedo of the cloud. It is this increase in the albedo of the cloud due to the presence of aerosols that is the first indirect aerosol effect.

As described in Twomey (1977) and Albrecht (1989), the second indirect effect states that the presence of aerosols will increase the liquid water content (LWC) of a cloud through the suppression of drizzle formation. Through an increase in LWC, aerosols will likely increase cloud top height and cloud lifetime (Forster and Ramaswamy 2007). The mechanism behind the suppression of rain relates to the collision-coalescence process. If the amount of liquid water is held constant within

a given cloud layer, cloud droplets in a polluted air mass will be smaller than in a clean air mass. This reduces the efficiency of the collision-coalescence process within clouds because the efficiency of this process largely depends on the radius of the largest cloud drops. Jonas (1996) explains that the initial formation of drizzle requires coalescence of cloud droplets since growth by condensation is too slow of a process. In that study the critical effective radius was roughly 20 μm. In a more recent study, Rosenfeld et al. (2012) found that this critical effective radius is 12-14 μm. The absence of large cloud drops in polluted air masses leads to a reduced efficiency in the drizzle formation process. This leads to a decrease, and in extreme cases, complete suppression, of the precipitation in a given cloud. Since the cloud is no longer precipitating efficiently, the cloud lifetime will increase. The increased liquid water content and increased cloud lifetime allow for increased latent heat release within the cloud. This makes the cloud more buoyant, increasing the cloud top height (Kaufman et al. 2005; Pawlowska and Brenguier 2003).

Bennartz (2007) found that maximum cloud droplet number concentration (CDNC) values are found over the continents and minimum CDNC values are found out over the open ocean. An increase in CDNC may also lead to suppression of precipitation as seen in boundary layer clouds when moving from the open ocean towards the coastline. An increase in CDNC is the result of a gradient in aerosols where aerosol concentration increases closer to lind compared to open ocean. Thus far, the only global evidence of the second indirect aerosol effect has come from modeling studies

where the evidence points to the suppression of precipitation in areas of high aerosol loading (e.g. Jacobson et al. 2007; Jiang et al. 2002; Lu and Seinfeld 2005).

From a global study involving satellite datasets and a global transport model, L'Ecuyer et al. (2009) found a more complex relationship between aerosols and precipitation suppression. First, if the aerosols were mostly made up of sulfate particles, then precipitation suppression did indeed occur. However, if the aerosols had a larger concentration of sea salts, then the opposite effect was seen as precipitation was enhanced because sea salts are typically larger than sulfate particles. As a result, sea salts can provide a source for embryonic raindrops, accelerating the precipitation process and decreasing cloud lifetime as a consequence. Therefore, the effect aerosols have on precipitation is not only a factor of aerosol loading but of the composition of the aerosols as well. If sulfates are more abundant, precipitation may be suppressed, and if sea salts are more abundant precipitation may be enhanced. Warm clouds (clouds from this point on) with low LWP values will not precipitate in most instances regardless of aerosol load while clouds with high LWP values would need exceptionally large CDNC values to suppress precipitation. However, clouds with moderate (250-375 gm^{-2}) liquid water path (LWP) values are most susceptible to changes in aerosol loading. It was also noted that there is evidence of a reduction in drizzle drop concentration within marine stratocumulus cloud decks in certain places. Out in the open ocean, the only process that could account for a reduction in drizzle in such a specific area is the increase in aerosol

load as a result of emissions from ships.

From an *in situ* field study, Pawlowska et al. (1999) also found that precipitation efficiency is more likely to be higher in a clean marine air mass than in a polluted air mass. In addition, Pawlowska and Brenguier (2003) found that drizzle is reduced at a rate proportional to H^3/N where H is the geometric thickness of the cloud and N is CDNC. Geometric thickness is a measure of how thick a cloud would be if it were completely homogeneous. In shallow stratiform clouds, variations in CDNC are more important in determining precipitation efficiency than variations in geometric thickness because these clouds are really shallow regardless of CDNC concentration. Bennartz (2007) utilized this relationship to define a drizzle threshold. Areas where drizzle was likely to be occurring was defined to be where $\frac{H^3}{N} > 0.4$. Depending on the relationship used, this ratio corresponds to drizzle rates between 0.5 mm/day and 2.5 mm/day.

Other studies have defined a drizzle threshold using another satellite-derived parameter, effective radius. Painemal and Zuidema (2011) concluded that drizzle could be identified from MODIS effective radius retrievals. Using the standard 2.1 μm wavelength effective radius retrieval, a threshold for precipitation onset was found to be when the effective radius is around 12 μm. A 12 μm threshold corresponds to radar reflectivity values between -19 dBz and -15 dBz. These values are consistent with drizzle onset found in multiple studies (e.g. Chin et al. 2000; Frisch et al. 1995; Liu et al. 2008; Wang and Geerts 2003). The drizzle threshold

found by Frisch et al. (1995) utilized a K_α-band radar (8.66 mm wavelength) while Chin et al. (2000) and Wang and Geerts (2003) utilized a W-band radar (3 mm).

The direct aerosol effect, semi-direct aerosol effect, and two indirect aerosol effects are important areas of climate research because the single largest source of uncertainty when evaluating climate forcing is aerosols effects. The uncertainty in the cloud albedo effect is 1.5 W/m^2. The cloud albedo effect is also known as the first indirect effect and is described above. The next largest uncertainty is only 0.8 W/m^2 from the direct aerosol effect. These are significant because the largest uncertainty from a forcing not related to aerosols is only 0.4 W/m^2 for the change in surface albedo due to land use and changes in tropospheric ozone concentration (Forster and Ramaswamy 2007).

Multiple studies (Kaufman et al. 2005; L'Ecuyer et al. 2009; Rosenfeld 2000) have shown that the various aerosol effects described above have a noticeable impact on cloud formation and precipitation efficiency. Consistent with the indirect effects, these studies have found that an increase in aerosol concentration leads to an increase in CDNC and a decrease in effective radius. The decrease in effective radius then leads to precipitation suppression, as the cloud drops are not large enough for the initiation of the collision-coalescence process. Furthermore, Kaufman et al. (2005) found that not only does an increase in aerosol concentration lead to precipitation suppression, but also to a systematic increase in cloud cover. The increased cloud cover is the result of increased cloud condensation nuclei in pristine

marine air where cloud formation would be extremely difficult. Increased aerosol concentration led to more cloud formation closer to the African coast in a region characterized by biomass burning. In another study, Wu et al. (2013) found that by acting as CCN, aerosols can decrease cloud droplet size and lower precipitation efficiency within the monsoon rains in East Asia. Bennartz et al. (2011) found that pollution from China increases CDNC and suppresses rain over the East China Sea.

Another study, Costantino and Breon (2013), found that the cloud droplet radius-cloud optical thickness relationship is positive for non-precipitating clouds and negative for precipitating clouds. In addition, for large aerosol index values, the cloud droplet radius is 3-5 μm smaller than in clean conditions. Interestingly, for the clouds they studied, they found that thin liquid clouds have smaller liquid water path values in the presence of polluted atmospheric layers while thick liquid clouds have larger liquid water paths. With these results, the authors concluded that the impact of aerosols on cloud microphysics is strong.

Using the Tropical Rainfall Measuring Mission (TRMM) satellite, Rosenfeld (2000) found clear evidence that smoke from biomass burning events suppresses precipitation. Furthermore, "pollution tracks" were found to also have reduced precipitation. "Pollution tracks" are defined to be tracks of pollution clearly evident in satellite imagery. Most pollution tracks are located downwind of point sources of pollution, such as power plants and major population centers. Within a given air

mass, clouds in the pollution tracks had reduced or suppressed precipitation, while clouds outside of the pollution track did not experience reduced or suppressed precipitation. Various measurements taken from TRMM indicate that the lack of precipitation within pollution tracks was not the result of an air mass change or any other meteorological process. The precipitation suppression within pollution tracks is consistent with the precipitation suppression seen within ship tracks. Both pollution and ship tracks provide valuable evidence supporting the hypothesis that increased aerosol concentrations lead to precipitation suppression through the processes described by the different aerosol effects.

The objective of this study is two-fold. First, the primary objective is to identify observational challenges in assessing the aerosol indirect and semi-direct effect. A secondary objective is to use observations to further test the hypothesis that aerosol concentration leads to precipitation suppression by focusing on precipitation efficiency in stratiform warm clouds in the South Atlantic Ocean off the west coast of Africa.

The study region is defined to be between 5°S and 25°S and 10°W and 15°E (Figure 1.1). This region is an ideal region to study the effects of aerosols on precipitation efficiency due to large but periodic sources of aerosols in this region due to biomass burning. The biomass burning season in Africa's southern half ranges from May through October, with a peak in the area of study occurring in the latter half of the season, or about July through October. As the season progresses, shrub land and

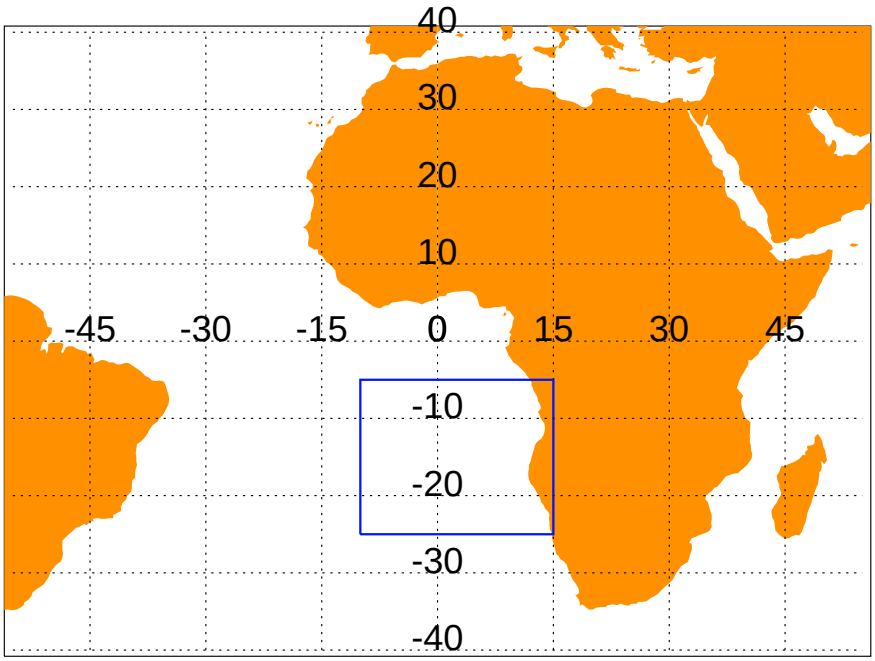

FIGURE 1.1: Map of study area outlined in blue.

grassland become the dominant fuel types (Roberts et al. 2009). The presence of biomass burning leads to the transport of large amounts of aerosols into the South Atlantic Ocean as a consequence of the prevailing easterly winds in the subtropics. Aerosols from biomass burning are usually trapped below 3km, the height of the inversion that typically is found in this part of the tropics and subtropics. As a result, smoke particles will be able to act as CCN in warm clouds (Crutzen and Andreae 1990).

Chapter 2

Instruments and Datasets

2.1 CALIOP

The Cloud-Aerosol LIdar with Orthogonal Polarization (CALIOP) instrument is a dual-wavelength polarization-sensitive lidar operating aboard the Cloud-Aerosol Lidar and Infrared Pathfinder Satellite Observations (CALIPSO) satellite. CALIPSO flies as a part of the NASA A-TRAIN constellation of satellites, which is in sun synchronous orbit with a 1:30pm local time equator crossing. CALIOP operates at 532 nm and 1064 nm at a high resolution of 30-60 m vertically and 333 m horizontally. CALIOP is sensitive to the presence of aerosols as well as cloud top height as a result of the high resolution and wavelengths chosen. The 532 nm channel operates with two orthogonally polarized components, perpendicular and parallel.

The dual-polarization data allows for a more robust determination of many aerosol variables, including aerosol type, orientation, and shape. In addition to the attenuated backscatter and vertical feature mask defined below, cloud top height (CTH) is also retrieved from CALIOP.

2.1.1 Attenuated Backscatter

The 1064 nm channel attenuated backscatter product (units of km^{-1} sr^{-1}) is a part of the LIDAR Level 1 Data products. The 1064 nm channel attenuated backscatter is used instead of the 532 nm channel as there is less noise in this band since it is further from the wavelength of maximum emission of the sun (482 nm assuming a temperature of 6000 K). The 1064 nm attenuated backscatter has a nominal range of 0.0 to 2.0 km^{-1} sr^{-1} and is reported at 583 levels in the vertical profile.

2.1.2 Vertical Feature Mask

The vertical feature mask is a LIDAR Level 2 Data product. The vertical feature mask classifies every data point, both vertically and horizontally, into one of seven classification types: clear air, cloud, aerosol, stratospheric layer, surface, subsurface, and totally attenuated (Powell and Vaughan 2013). Every point identified as either cloud or aerosol is then further subtyped. Clouds can be subtyped into four categories and aerosol can be subtyped into six categories (Table 2.1). Three of

Cloud	**Aerosol**
Unknown	Clean Marine
Ice	Dust
Water	Polluted Continental
Oriented Ice	Clean Continental
	Polluted Dust
	Smoke

TABLE 2.1: Cloud and aerosol subtyping categories.

these aerosol classes (dust, smoke, and polluted continental) have the same physical and optical characteristics that the AERONET network (a global network of multi-wavelength sun photometers used to make sky radiance measurements and inversions of aerosol microphysical properties) uses for its aerosol type classification. The vertical feature mask is reported at 545 levels in the vertical profile. Additionally, the vertical resolution changes from 30 m in the lowest 8 km to 60 m for the next 12 km, and, finally, to 180 m from about 20 km to 30 km in altitude.

2.2 CloudSat-Cloud Profiling Radar

The Cloud Profiling Radar (CPR) is a near nadir pointing cloud radar operating at 94 GHz (3.19mm, W-band). CPR has a vertical resolution of only 500 m and an along track horizontal resolution of 1.7 km. CPR has 125 levels in the vertical, with 105 levels located above mean sea level. CPR is ideally suited to study drizzle and precipitation efficiency due to its low minimum detectable reflectivity of -29

dBZe. CPR currently flies on the CloudSat satellite, which was launched in 2006. CloudSat flies as a part of NASA's A-TRAIN.

2.2.1 Level 2 Data

The reflectivity profile from CPR is used to help monitor the precipitation efficiency within the stratocumulus clouds in this region. However, the light drizzle that this study focuses on cannot be reliably detected below roughly 1 km because the outgoing radar pulse not a perfect square wave, thereby increasing the surface clutter in the data up to roughly 1 km above the surface (Marchand et al. 2008).

2.2.2 2C-PRECIP-COLUMN

The 2C-PRECIP-COLUMN product estimates the occurrence of precipitation and its intensity at the surface. The precipitation flag indicates the presence of precipitation using CPR reflectivity as a basis for this determination. There are four possible values for this flag: 0-no precipitation detected, 1-rain possible, 2-rain probable, and 3-rain certain. Roughly speaking, the rain possible flag corresponds to reflectivity values greater than -15 dBZ, the rain probable flag corresponds to reflectivity values greater than -7 dBZ, and the rain certain flag corresponds to

reflectivity values greater than 0 dBZ. This study utilizes the status flag in conjunction with the precipitation flag. The status flag reports if the retrieval successfully determined the incidence and intensity of precipitation, just the incidence of precipitation, or if there was an error in the retrieval. The following is a list of reasons an error could have occurred: reflectivity profile bad, gaseous attenuation missing, sea surface temperature missing, surface wind speed missing, σ_0 (surface attenuated backscatter cross section) could not be determined, cloud base could not be determined, near surface reflectivity missing, or freezing level could not be determined.

2.3 MODIS

The MODerate resolution Imaging Spectroradiometer (MODIS) is an imaging instrument with 36 spectral bands covering the entire solar and terrestrial infrared spectral range. MODIS has roughly a 1 km spatial resolution, but this is dependent on which band is used. MODIS flies aboard two Earth Observing System satellites, Aqua and Terra. For this study, the MODIS instrument aboard Aqua was used. As with CloudSat and CALIPSO, Aqua is flown in NASA's A-TRAIN.

2.3.1 Cloud Parameters

This study utilizes the Level 2 MODIS cloud products subset along the CloudSat field of view track. This dataset contains cloud optical and microphysical properties including: cloud top temperature (CTT), cloud top pressure (CTP), cloud optical depth (COD), and effective radius. These products are derived from varying combinations of the 36 spectral bands that make up MODIS.

2.3.2 Level-3 Daily Global Gridded Data

Aerosol optical depth from the MODIS Level 3 daily global gridded data at 1°x1° resolution is used as an alternative method to calculate column averaged atmospheric aerosol concentration. This product is derived from the Level 2 atmosphere products. The statistics for each science parameter are then aggregated onto a 1°x1° equal-angle global grid.

Chapter 3

Evaluation Methods

3.1 Scene Classification

The four-year (2007-2010) dataset used in this study is divided into three categories-rainy, cloudy, and clear-in order to isolate the effects of aerosols on precipitation efficiency. The scene classification requirements can be found in Table 3.1. Some requirements, such as cloud top height greater than or equal to 0 km in the clear classification, are used to ensure that the data used are valid for a column. The cloud top temperature requirement of 253 K to allow for supercooled water to be present in the cloud. Increasing the cloud top temperature to 273 K makes only a minor difference in the number of columns identified as there are only 287 rainy or cloudy columns that have a cloud top temperature below 273 K. This most

	Rain	**Cloud**	**Clear**
MODIS:	CTT greater than 253 K	CTT greater than 253 K	
	COD greater than 3	COD greater than 3	COD less than 0
	Effective radius greater than 0 μm	Effective radius greater than 0 μm	
2C-PRECIP-COLUMN:	Precip Flag: 1-Rain Possible 2-Rain Probable 3-Rain Certain	Precip Flag: 0-No Precipitation Detected	Precip Flag: 0-No Precipitation Detected
	Status Flag: 0-Both quantitative precip rate and occurrence retrievals were successful 1-Only the precip occurrence retrieval was successful; no precip rate was retrieved		
CALIOP:		Vertical Feature Mask-Feature Type: 2-Cloud	Vertical Feature Mask-Feature Type: 0-Invalid (bad or missing data) 1-Clear Air 3-Aerosol 5-Surface 6-Subsurface 7-No signal (totally attenuated)
		Feature Type-Quality Assurance: 2-Medium 3-High	Feature Type-Quality Assurance 0-None (used for clear air feature type) 2-Medium 3-High
	CTH greater than or equal to 1 km	CTH greater than or equal to 1 km	CTH equal to 1 km
	CTH less than or equal to 5 km	CTH less than or equal to 5 km	

TABLE 3.1: Scene classification requirements.

likely is the case because the cloud top height requirement of 5 km or less is the limiting factor on what the cloud top temperature can be in most instances. The focus of this study is limited to warm clouds, unlike Rosenfeld (2000), because warm clouds are easier to constrain. Cold clouds have more constraints as not all particles that act as CCN can act as nuclei in ice clouds. Another complication is that the efficiency of cold cloud processes is a function of temperature, becoming

more efficient as the temperature drops. Peak efficiency is between -10° and -20°C (Cotton et al. 1986). Cold clouds also have interfering processes that make them harder to analyze. Using the classification scheme just described, our dataset has 31,692 rainy columns, 162,950 cloudy columns, and 262,115 clear columns. The data is then further classified by the presence of an aerosol layer above cloud top, as identified by the CALIOP VFM. Once the columns with aerosol layers are identified, the difference between cloud top height and aerosol base height is determined. If this difference in height is less than 250 m, the column is identified as having an aerosol layer touching the cloud. Otherwise, the column is identified as having an aerosol layer above the cloud. Out of the 31,692 rainy columns identified, 8,067 columns have an aerosol layer, of which 669 are touching and 7,398 are above the cloud. Out of the 162,950 cloudy columns, 45,930 have an aerosol layer above the cloud with 8,855 columns having an aerosol layer touching and 40,075 columns having an aerosol layer above the cloud. Out of the 262,115 clear columns, 30,884 have an aerosol layer in the column.

3.2 Aerosol Concentration

3.2.1 Vertically Integrated Attenuated Backcatter

3.2.1.1 Methods

As a proxy for aerosol optical depth, the 1064 nm channel attenuated backscatter and the vertical feature mask are used to measure aerosol concentration within an atmospheric column. First, the vertical feature mask is used to locate aerosol layers that are above cloud top or above 1 km in the absence of clouds. Once the aerosol layers are identified in the column, the 1064 nm attenuated backscatter is used in a variety of ways to calculate aerosol concentration. The eight calculations that will be discussed in this section are: clear sky integrated boundary layer backscatter (total), $CLEARTOT$; clear sky integraged elevated boundary layer backscatter (elevated), $CLEARVIAB$; clear sky integrated surface boundary layer backscatter (low), $CLEARLOW$; clear sky integrated aerosol boundary layer backscatter (total aerosol), $CLEARTOTAER$; clear sky integrated elevated aerosol boundary layer backscatter (elevated aerosol), $CLEARAERVIAB$; clear sky integrated surface aerosol boundary layer backscatter (low aerosol), $CLEARLOWAER$; integrated elevated boundary layer backscatter (rain/cloud total), $VIAB$; and integrated elevated aerosol boundary layer backscatter (rain/cloud aerosol), $AERVIAB$. The last two aerosol parameters will have a slightly different interpretation than the first

six aerosol parameters. The first aerosol parameter, clear sky integrated boundary layer backscatter, is calculated according to the following equation:

$$CLEARTOT = \int_{z=0m}^{z=5000m} \sigma_b \mathrm{d}z, \tag{3.1}$$

where σ_b is the attenuated backscatter at 1064 nm and CLEARTOT has units of sr^{-1}. The second aerosol parameter, clear sky integrated elevated boundary layer backscatter, is calculated as follows:

$$CLEARVIAB = \int_{z=1000m}^{z=5000m} \sigma_b \mathrm{d}z. \tag{3.2}$$

The third aerosol parameter, clear sky integrated surface boundary layer backscatter, is calculated according to the following equation:

$$CLEARLOW = \int_{z=0m}^{z=1000m} \sigma_b \mathrm{d}z. \tag{3.3}$$

The fourth aerosol parameter, clear sky integrated aerosol boundary layer backscatter, is calculated as follows:

$$CLEARTOTAER = \int_{z=0m}^{z=5000m} \sigma_b (VFMFT = 3) \mathrm{d}z, \tag{3.4}$$

where $VFMFT = 3$ is the vertical feature mask-feature type that corresponds to aerosol. The fifth aerosol parameter, clear sky integrated elevated aerosol boundary

layer backscatter, is calculated according to the following equation:

$$CLEARAERVIAB = \int_{z=1000m}^{z=5000m} \sigma_b(VFMFT = 3)\mathrm{d}z. \tag{3.5}$$

The sixth aerosol parameter, clear sky integrated surface aerosol boundary layer backscatter, is calculated as follows:

$$CLEARLOWAER = \int_{z=0m}^{z=1000m} \sigma_b(VFMFT = 3)\mathrm{d}z. \tag{3.6}$$

The first three aerosol parameters integrate through all layers, while the last three parameters only integrate through layers identified as aerosol by the vertical feature mask. The clear sky integrated boundary layer backscatter and clear sky integrated aerosol boundary layer backscatter integrate from 5000m to the surface. The integration begins at 5000 m because the atmosphere above this level should not influence the low-level stratocumulus clouds that are the focus of this study. The clear sky integrated elevated boundary layer backscatter and clear sky integrated elevated aerosol boundary layer backscatter integrate between 5000 m and 1000 m. Sea salt should influence these two parameters less than the first two parameters described. This is a useful distinction, as the focus of this study is on biomass burning aerosols being transported over the stratocumulus clouds, not the sea salt aerosols that are always present. The last two parameters, clear sky integrated

surface boundary layer backscatter and clear sky integrated surface aerosol boundary layer backscatter, are calculated only through the lowest 1000 m. This, again, is done to try and isolate the effects of sea salt from that of the biomass burning aerosols.

These six aerosol parameters are only calculated in columns identified as clear sky, according to the classification scheme previously described. The parameters are then separated into 1°x1° bins and averaged. The average aerosol concentration is calculated daily. Once the data is binned, it is co-located with the rainy and cloudy pixels. Each rainy and cloudy pixel is assigned an aerosol concentration based on the 1°x1° bin in which it was located. This aids in assessing the relationship between aerosol concentration and various cloud macro- and micro- physical properties.

The final two aerosol parameters, integrated elevated boundary layer backscatter and integrated elevated aerosol boundary layer backscatter, are calculated as follows:

$$VIAB = \int_{z=z_{bot}}^{z=5000m} \sigma_b \mathrm{d}z, \text{and} \tag{3.7}$$

$$AERVIAB = \int_{z=z_{bot}}^{z=5000m} \sigma_b (VFMFT = 3) \mathrm{d}z, \tag{3.8}$$

where $z_{bot} = 1000$ m in the absence of clouds or if the cloud top height is below 1000 m, or $z_{bot} = CTH + 90$ m in the presence of clouds. The purpose of integrating

to 90 m above cloud top is to avoid integrating through the cloud layer, as this would drastically increase the vertically integrated attenuated backscatter for that column. Furthermore, given the wavelengths that CALIOP operates at, the signal becomes rapidly attenuated in the presence of clouds. Contrary to the first six aerosol parameters, these last two parameters are only calculated for columns where a cloud (rain or cloud column) is detected. As a consequence, these two parameters do not need to be binned, averaged, and co-located in order to be matched up with cloud properties. Additionally, these last two aerosol parameters can no longer be compared to the MODIS aerosol parameters as they are no longer looking at the same scene. This will be discussed in the following sections.

3.2.1.2 Results

Figure 3.1 shows the results of the six clear sky calculations as a monthly average for the combined dataset of rain and cloud column identification. The magnitude of each calculation relative to the other calculations is consistent with expectations; total is greater than elevated which is greater than low, and total aerosol is greater than both elevated aerosol and low aerosol. The only relative magnitude that may be somewhat surprising is that the low aerosol is greater than the elevated aerosol for January-March and October-December. This would lead one to believe that outside the biomass burning season there is little aerosol transported above the stratocumulus cloud layer. Interestingly, total appears to have three maxima,

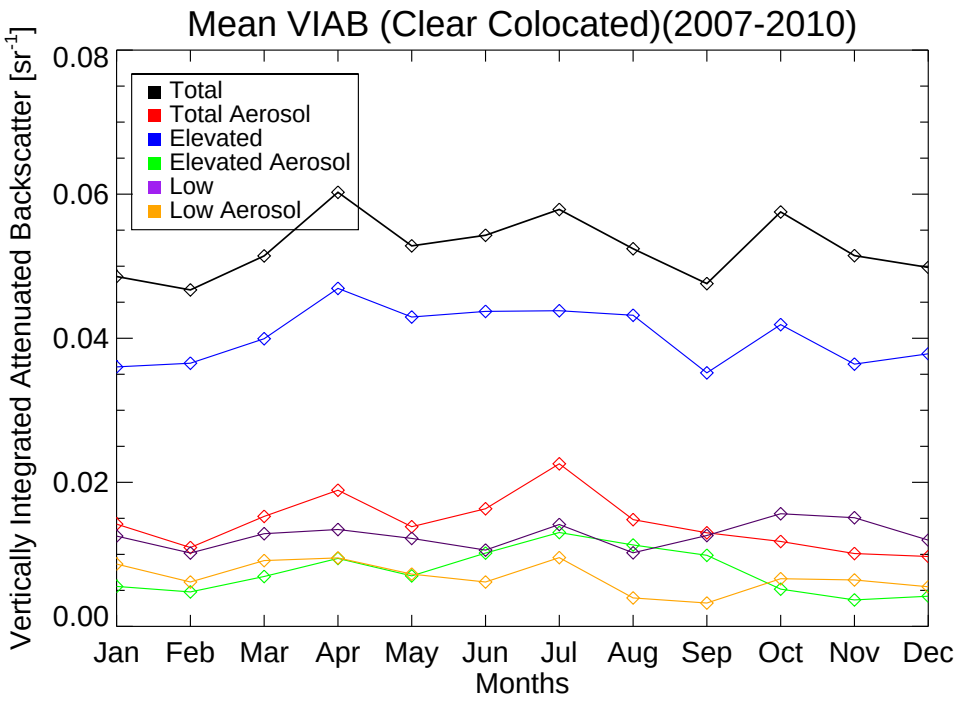

FIGURE 3.1: Monthly average of the six 1064 nm Clear Sky Vertically Integrated Attenuated Backscatter (sr^{-1})(VIAB) calculations for 2007-2010. Total is the integration from the surface to 5 km, Total Aerosol is the integration from the surface to 5 km integrating only through aerosol layers, Elevated is the integration from 1 km to 5 km, Elevated Aerosol is the integration from 1 km to 5 km integrating only through aerosol layers, Low is the integration from the surface to 1 km, and Low Aerosol is the integration from the surface to 1 km integrating only through aerosol layers.

April, July, and October. All three months are somewhat surprising. While July and October are within the biomass burning season, they are at the beginning and end of the season, not when one would expect the season to be strongest. The April peak in total appears to be the result of a peak in the elevated curve during the same month. Elevated appears to be the dominant contributor to the total concentration. The low concentration does account for the peak in the total concentration in July and October, however. It is unclear why there is a peak in low

level backscatter during these months. Total aerosol appears to follow the trend of low aerosol outside of the biomass burning season and elevated aerosol during the biomass burning season, especially August and September. Therefore, it appears that more aerosol is being transported into the region during the biomass burning season. Interestingly, however, the biggest peak in total aerosol occurs in July, when both low aerosol and elevated aerosol have a maximum. Total aerosol also does not appear to make up a large portion of the total backscatter.

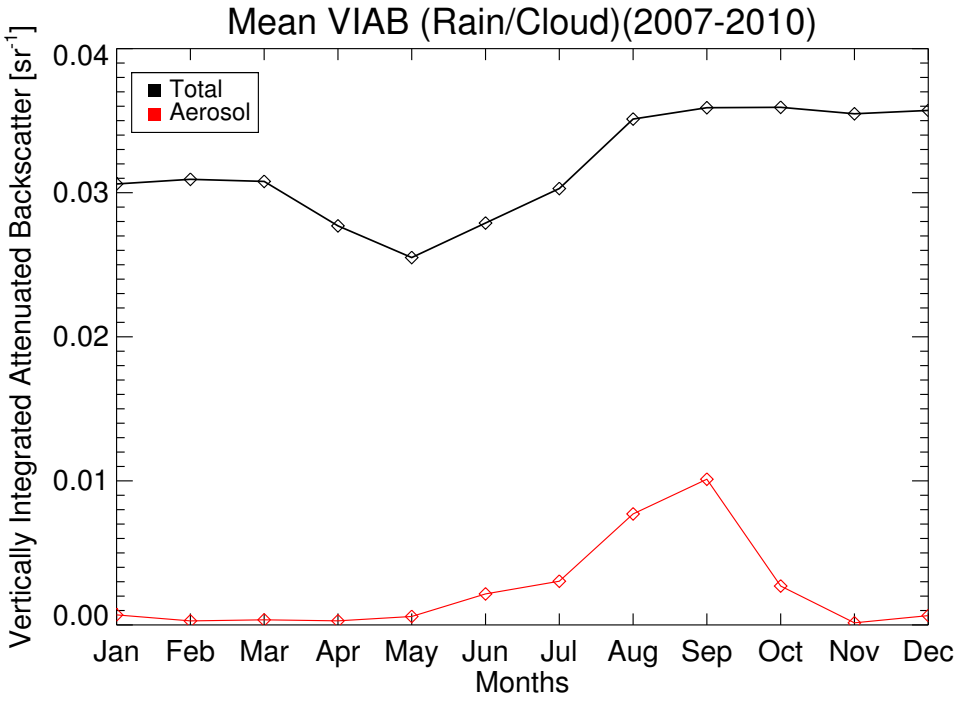

FIGURE 3.2: Monthly average of the two 1064 nm Vertically Integrated Attenuated Backscatter (sr^{-1})(VIAB) calculations for 2007-2010. Total is the integration from $z = z_{bot}$ to 5 km, Aerosol is the integration from $z = z_{bot}$ to 5 km integrating only through aerosol layers.

Figure 3.2 shows the result of the two aerosol calculations that were calculated from

the rainy and cloudy columns directly. Again, we see that the total is greater than aerosol. We see that the total from this figure is smaller in magnitude than the elevated from figure 3.1 and that aerosol is similar to elevated aerosol, especially during the biomass burning season. Unlike elevated and elevated aerosol, though, total and aerosol from the rain/cloud identification do experience a maximum during the biomass burning season, as would be expected.

As mentioned above, it appears that more aerosol, namely smoke, is being transported during the biomass burning season and that the percentage of aerosol that may be attributed to sea salt is larger outside the biomass burning season. To see if this is the case, the lowest aerosol layer that is above cloud top or above 1 km in the absence of clouds, what we will now call the base aerosol layer is identified using the CALIOP vertical feature mask. The composition of the base aerosol layer, as determined by this method, is shown in Figure 3.3. This figure shows the percentage of base aerosol layers that fall into each classification. The rest of the bar plot, from the top of the dust classification to 100%, is aerosol identified as clean marine or sea salt. This plot shows an increase in smoke as the base aerosol type as we progress through the biomass burning season. The increase in smoke occurs with a reduction in clean marine aerosol, as the other aerosol types remain fairly constant year round. This fits with the aerosol type expected based on both the region and the analysis above. As most of the dataset is comprised of clear air, there is a bias towards the clean marine aerosol identification. In clear air the base

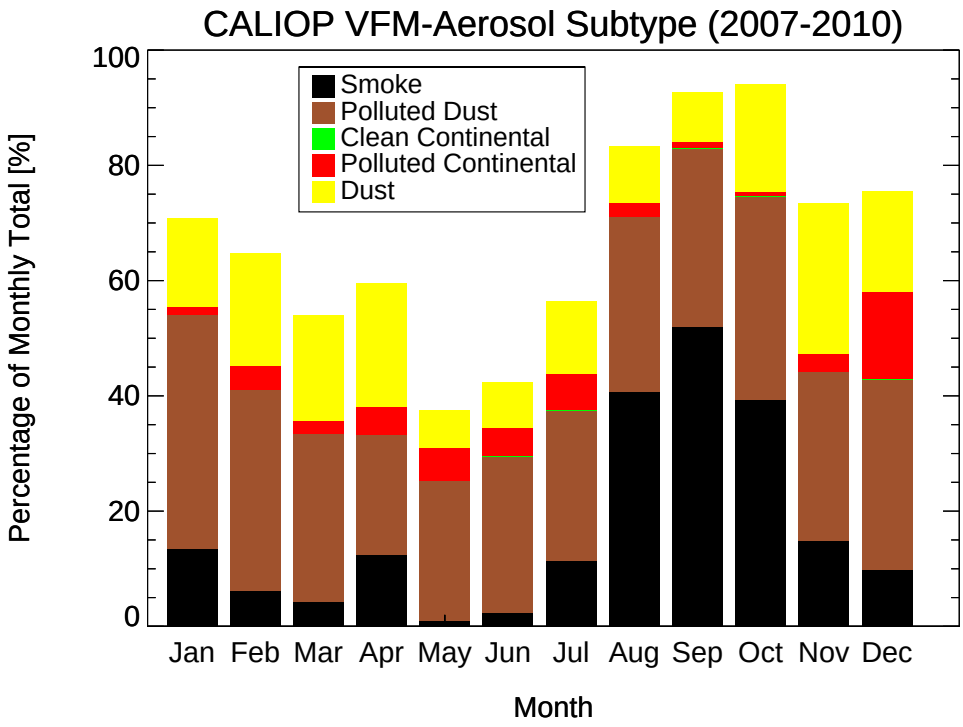

FIGURE 3.3: Base aerosol layer aerosol subtype by percentage of total per month for the entire dataset. From the top of the dust bar to 100% is clean marine aerosol.

aerosol layer is most likely at the 1 km lower threshold. At this level, we would expect an abundance of clean marine aerosol when out over the ocean. In order to reduce the bias towards clean marine aerosol, the same plot was created from the combined dataset of the rain and cloud column identification (Figure 3.4). In this figure the increase in smoke during the biomass burning season is even more evident. The increase in smoke appears to be at the expense of both clean marine aerosol and dust. As another check to see if the signal in the vertically integrated attenuated backscatter calculation is correct, it is then compared with the MODIS derived aerosol optical depth.

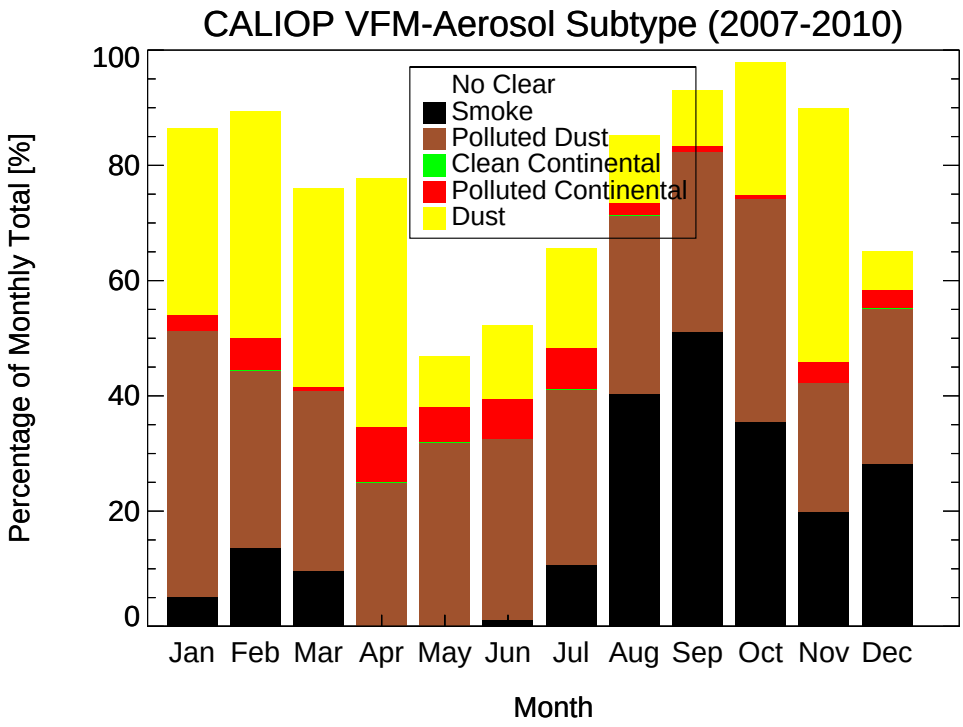

FIGURE 3.4: Base aerosol layer aerosol subtype by percentage of total per month for rain and cloud columns only. From the top of the dust bar to 100% is clean marine aerosol.

3.2.2 MODIS Aerosol Optical Depth

In order to use the MODIS Aerosol Optical Depth data, it first has to be co-located with all columns identified as either rainy or cloudy. Once this is done the monthly average aerosol optical depth can be calculated (Figure 3.5). It is important to note that a one-to-one comparison cannot be done between AOD and the other eight aerosol metrics as the units are not consistent between the CALIOP vertically integrated attenuated backscatter (sr^{-1}) and MODIS aerosol optical depth (none). With this in mind, the agreement in shape between AOD and

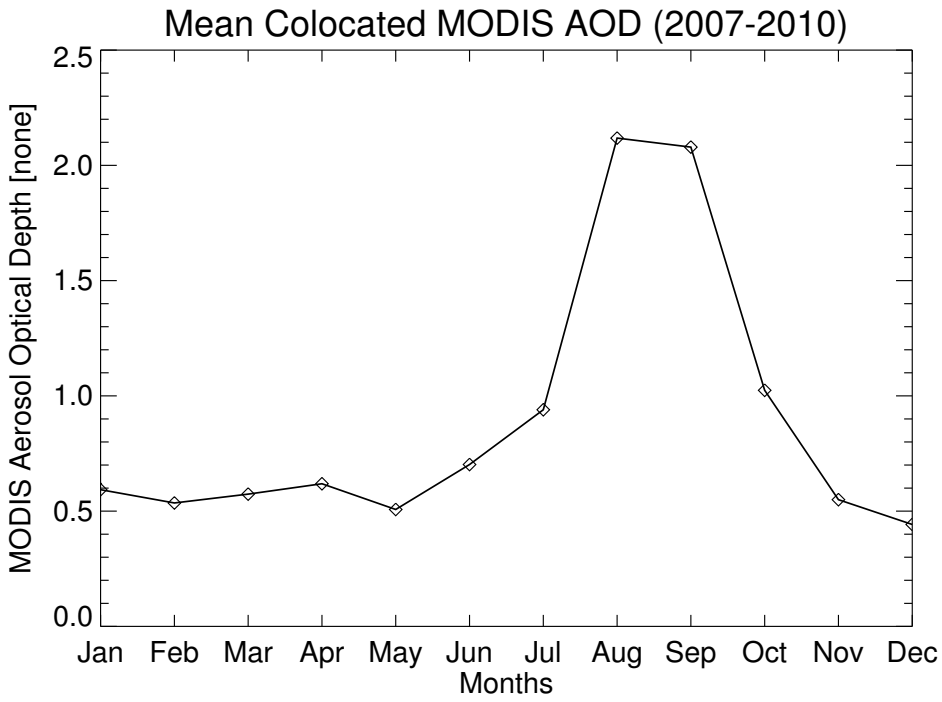

FIGURE 3.5: Monthly average 1°x1° MODIS Aerosol Optical Depth co-located with all rainy and cloudy columns in the dataset for 2007-2010.

the six clear sky aerosol metrics looks somewhat troublesome (Figure 3.1). MODIS AOD data shows a peak in aerosol concentration in August and September, much like rain/cloud total and rain/cloud aerosol, and elevated aerosol. With that being said, these three CALIOP aerosol metrics are three that MODIS AOD should correlate with the best. However, we would think that total and total aerosol would look more like MODIS AOD than they do. This is mostly a consequence of these two calculations having peaks in April and a minimum in September that the other aerosol metrics do not have. Since MODIS measures total column aerosol it makes sense that MODIS AOD would not agree with low and low aerosol as these

two calculations ignore most of the atmospheric column.

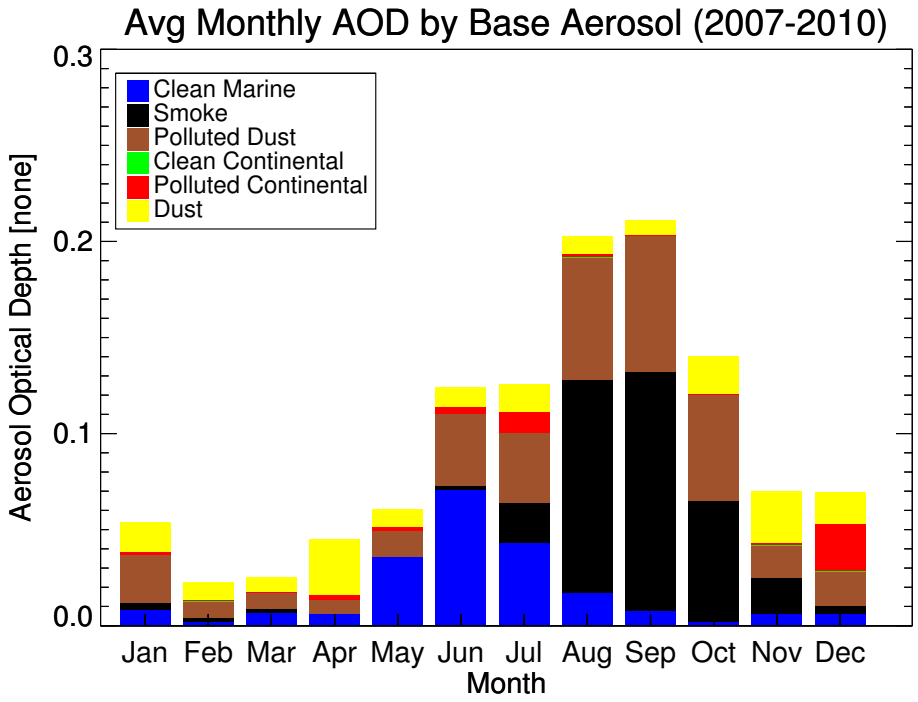

FIGURE 3.6: Monthly average MODIS AOD by base aerosol subtype for the entire dataset during the time period 2007-2010.

Given the discussion thus far, we would expect that the sharp increase in AOD during August and September would be the result of biomass burning and that most of the increase in AOD would be from smoke. To determine if this is the case, a similar method to the one used to determine the base aerosol layer is employed. The difference, however, is that in this case there is an extra step. Once the base aerosol layer is identified, the AOD associated with that column is assigned to that aerosol subtype. The average AOD associated with each aerosol subtype is plotted by month in figure 3.6. As we can see, the increase in MODIS AOD is a result of

an increase in smoke as the base aerosol subtype. This confirms that the increase in AOD is the result of the biomass burning season. As was the case with the base aerosol subtype, this figure may be biased toward clean marine as a majority of the dataset consists of clear columns. Monthly average MODIS AOD by subtype without the clear columns is shown in figure 3.7. The biggest difference is that

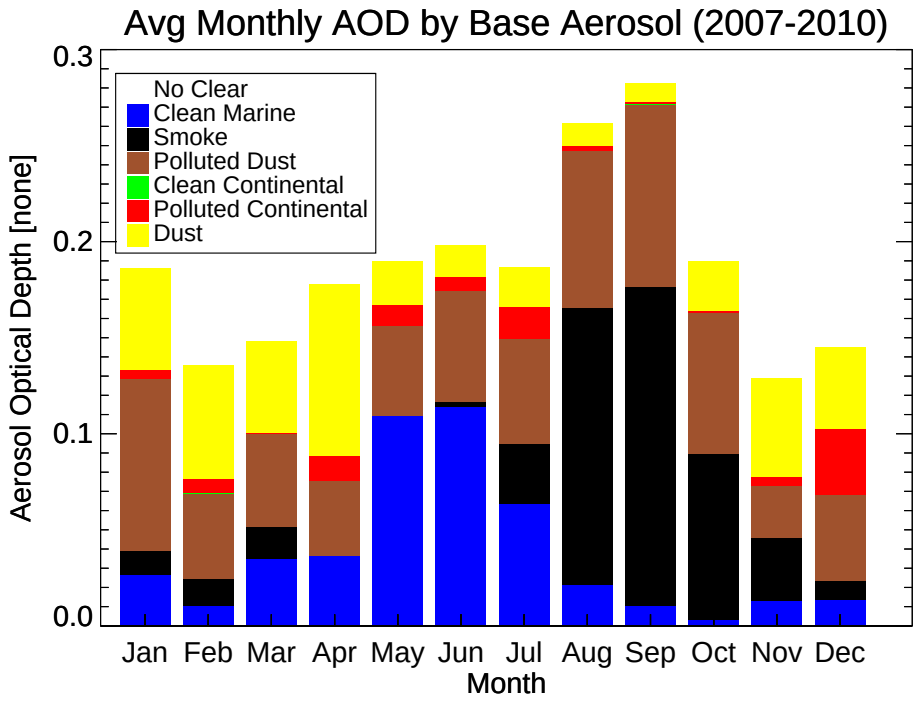

FIGURE 3.7: Monthly average MODIS AOD by base aerosol subtype for rain and cloud columns only during the time period 2007-2010.

the increase in smoke during the biomass burning season is even more evident in this case. The increase in average AOD is more complicated to explain as MODIS AOD is only calculated under clear sky conditions.

3.2.3 MODIS Aerosol Index

Before looking at the monthly average of MODIS Aerosol Index (AI), it is worthwhile to define what MODIS AI is. MODIS AI is similar to MODIS aerosol optical depth but is more sensitive to fine mode aerosols. This is because AI is the product of the AOD and angstrom exponent, $AI = AOD * AE$. The angstrom exponent is used to describe the dependence of aerosol optical depth on wavelength. AI, therefore, is more sensitive to fine mode aerosols as the angstrom exponent is larger for fine mode aerosols than coarse mode aerosols.

In order to use the MODIS AI data, it first had to be co-located with all columns identified as either rainy or cloudy, in the same was as MODIS AOD. Once this is done the monthly average aerosol optical depth can be calculated (Figure 3.8). MODIS AI looks very similar to MODIS AOD, the only difference is that the maximum in MODIS AI occurs in September as opposed to August. We also see that AI starts to increase in July, much like AOD, rain/cloud total, rain/cloud aerosol, and elevated aerosol.

3.2.4 Discussion

The 10 aerosol parameters used in this study all calculate an aerosol concentration in a different way and over different parts of the atmosphere. To begin with, the MODIS aerosol parameters only calculate aerosol concentration under clear sky

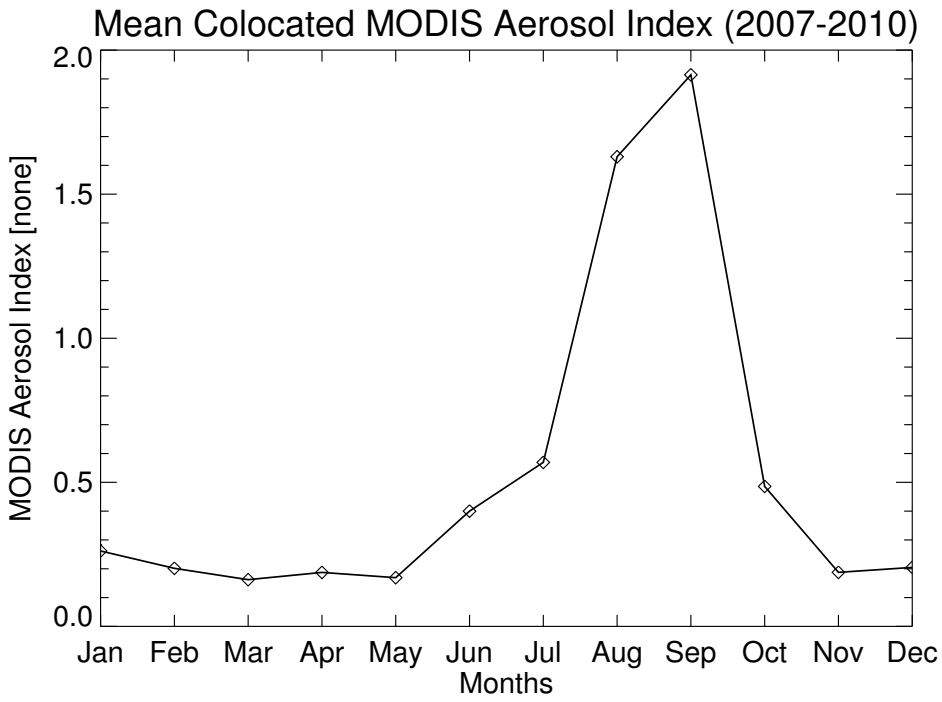

FIGURE 3.8: Monthly average MODIS Aerosol Index co-located with all rainy and cloudy columns in the dataset for 2007-2010.

conditions, meaning that aerosol concentration is not calculated in the presence of clouds. Even so, the MODIS aerosol parameters may still be subject to 3-D cloud effects and cloud contamination (Várnai and Marshak 2009; Wen et al. 2007; Zhang et al. 2005). With that being said, the advantage to MODIS is that it is an imager, and as such, has a much wider swath width than CALIOP since CALIOP is an active instrument. With the wider swath width MODIS has a greater chance of seeing clear sky in the area than CALIOP. This allows MODIS to calculate aerosol concentration over most of the area, especially when averaged into the 1°x1° bins used by the aerosol product in this study. The first six aerosol

parameters calculated from the CALIOP data (equations 3.1-3.6) utilize the clear sky identification. As a result, this data, especially when binned, can be directly compared to the MODIS data as all eight of the calculations only calculate aerosol concentration when looking at clear sky. This is in contrast to the last two aerosol parameters calculated from the CALIOP data (equations 3.7 and 3.8) which look at cloudy skies (both the rain and cloud classification). As a consequence these parameters cannot be compared directly with all the other aerosol parameters.

Since the integrated elevated boundary layer backscatter and integrated elevated aerosol boundary layer backscatter parameters are only calculated under cloudy conditions, they may be missing some of the aerosol. This is especially true in the cases when the aerosol layer is touching the cloud as a large portion of the aerosol concentration could be below or embedded within the cloud layer. In those cases the aerosol layers will not be calculated as the integration stops at cloud top height.

3.3 Vertical Distribution of Aerosols

Once the aerosol concentration and subtype is known, the next step is to identify the vertical distribution of the aerosols. In order to accomplish this two different calculations are used. The first calculation is the aerosol above cloud (AAC)

fraction. AAC is defined as

$$AAC = \frac{NAAC}{NAAC + CBNA}, \tag{3.9}$$

where $NAAC$ is the number of cases with aerosol above clouds and $CBNA$ is where there are clouds but no aerosol. In this case aerosol above clouds just means that there is an aerosol layer present, not that the aerosol layer is greater than 250 m above cloud top, as defined above. Therefore, this measure is used to determine when we are most likely to find an aerosol layer. The result of this is shown in figure

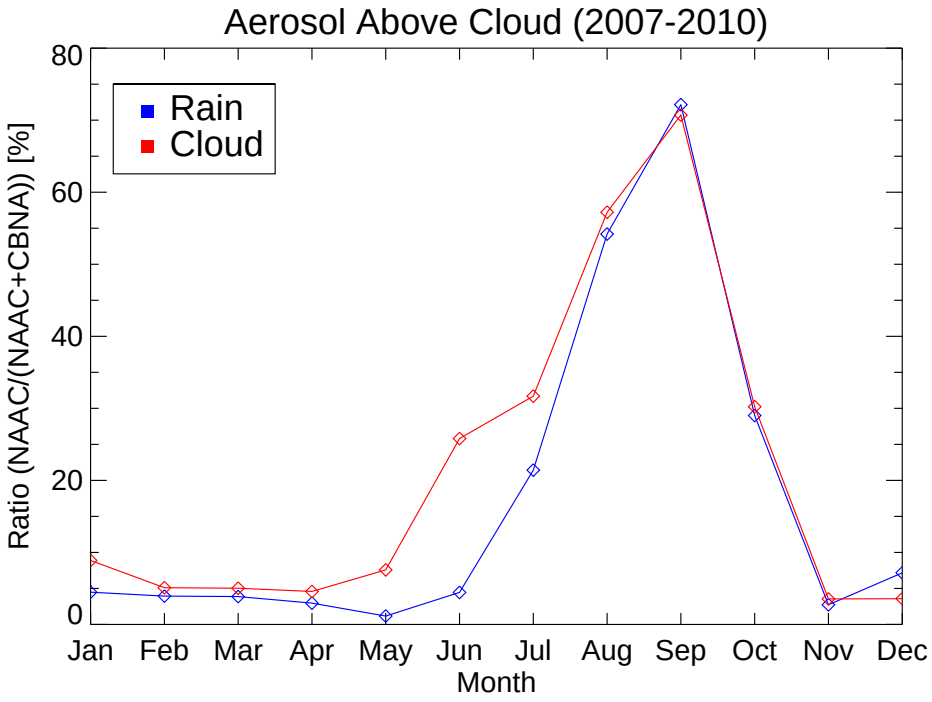

FIGURE 3.9: Monthly average aerosol above cloud fraction for 2007-2010.

3.9. First, AAC has roughly the same values for both the rainy and the cloudy

columns. Second, there is an increase of over 60%, from 5% to 70%, in AAC during the biomass burning season. Interestingly, the increase begins before the biomass burning season, in June for cloudy columns and July for rainy columns. This corresponds to when the AI and AOD concentrations began to increase as well.

The second calculation determines the percentage of aerosol columns that are touching the cloud. This equation is defined as

$$TOUCH = \frac{AER_{touch}}{AER_{touch} + AER_{above}}, \tag{3.10}$$

where AER_{touch} is the number of aerosol layers touching the cloud and AER_{above} is the number of aerosol layers above the cloud. Therefore, TOUCH is looking at where the aerosol layer is in relation to the cloud, as opposed to AAC which looked at the relation between the aerosol cases and no aerosol cases. The results of this calculation can be seen in figure 3.10. Unlike AAC, rainy and cloudy columns do not behave similarly throughout the year. They do, however, behave similarly for most of the biomass burning season, from July through October. What this shows us is that as the biomass burning season begins and smoke aerosols become more prevalent two things are happening. First, the number of aerosol layers above cloud top are increasing and, two, these aerosol layers are predominantly separated from the cloud layer and do not directly interact with the stratocumulus cloud field.

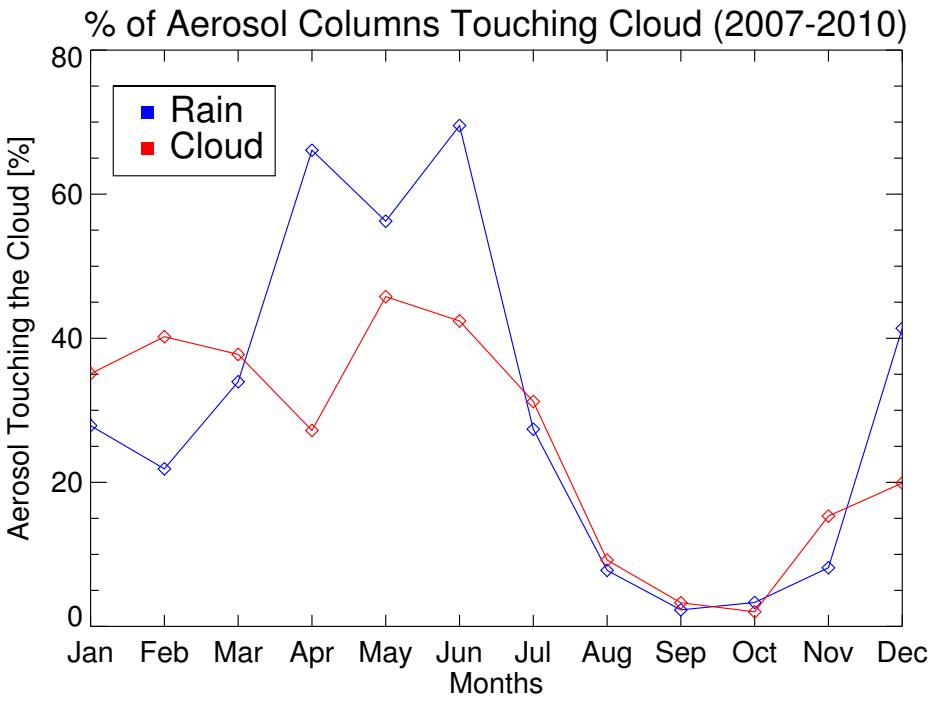

FIGURE 3.10: Monthly average aerosol touching cloud fraction for 2007-2010.

3.4 Cloud Droplet Number Concentration

CDNC (or N) is the concentration of activated CCN within a cloud. For this study, CDNC is calculated following the formula found in Bennartz (2007). The equation for CDNC is:

$$N = 2^{\frac{-5}{2}} \tau^3 \left(\frac{W}{C_F}\right)^{\frac{-5}{2}} \left(\frac{3}{5}\pi Q\right)^{-3} \left(\frac{3}{4\pi\rho_l}\right)^{-2} c_w^{\frac{1}{2}}, \tag{3.11}$$

where W is the cloud liquid water path for a vertically homogeneous cloud, c_w is the adiabatic condensation rate, C_F is the cloud fraction identified by MODIS, k is the ratio between volume mean radius and effective radius, τ is cloud optical depth, Q is scattering efficiency, and ρ_l is the density of water. For this study, k

and Q are assumed to be constant with values of 0.8 and 2 respectively. In addition, c_w is a function of CTT. *In situ* measurements of near cloud top LWC have been found to be near 80% of the adiabatic condensation rate. As a result, the above equations assume an 80% adiabatic condensation rate. Greater detail regarding subadiabatic stratocumulus cloud can be found in many papers (Albrecht et al. 1990; Bretherton et al. 2004). Lastly, W is defined as:

$$W = \frac{5}{9}\rho_l r_{eff}\tau, \tag{3.12}$$

where r_{eff} is the standard MODIS derived cloud droplet effective radius retrieval.

3.5 Geometrick Thickness

Geometric thickness (H) is a useful cloud macrophysical property. Together with CDNC, geometric thickness is a self-contained coordinate system for clouds. This is an alternative to the cloud effective radius/COD coordinate system that is widely used. Geometric thickness is also calculated following the formulas found in Bennartz (2007). The equation for H is:

$$H = (2\frac{W}{c_w C_F})^{\frac{1}{2}}, \tag{3.13}$$

where all the variables are the same as in equation 3.11 above.

3.6 Effective Radius

Effective radius is another useful cloud microphysical property. For this study, the effective radius product comes from the MODIS Collection 5 algorithms. Mathematically, effective radius is defined as the ratio of the third moment to the second moment of the cloud droplet size distribution:

$$r_e = \frac{\int_0^\infty \pi r^3 n(r) \mathrm{d}r}{\int_0^\infty \pi r^2 n(r) \mathrm{d}r}, \tag{3.14}$$

where $n(r)$ is the cloud droplet size distribution. However, in satellite based retrievals effective radius is determined based on the reflectances from two channels, one visible non-absorbing band, used mainly to calculate cloud optical depth (COD) and one from the near-infrared, a slightly absorbing band (Twomey and Seton 1980). The effective radius (and COD) are then determined using a look-up table, based on work done by Nakajima and King (1990). MODIS reports three different effective radius values based on three different channel combinations. All three channel combinations use the 0.86 μm channel for the visible channel. The three near- infrared channels used are 1.6, 2.1, and 3.7 μm where the 2.1 μm channel is used in the standard MODIS effective radius retrieval.

3.7 Precipitation Efficiency

As a measure of precipitation efficiency this study calculated a probability of precipitation (PoP) as a function of liquid water path. PoP is defined as:

$$PoP = \frac{RP}{RP + CP} * 100, \tag{3.15}$$

where RP is the number of precipitating cloud columns, CP is the number of non-precipitating cloud columns, and PoP is given as a percentage. In order to do this calculation the LWP values are first binned. Once binned, PoP is then calculated for each LWP bin. Additionally, the data is separated into four groups: above top, above bottom, touch top, and touch bottom. The above groups have aerosol layers above the cloud, whereas the touch groups have aerosol layers touching the clouds. The top and bottom groups are for the top and bottom 20% of aerosol cases respectively. This calculation is then carried out for all ten aerosol calculations presented earlier. Results of this calculation will be shown in Chapter 4.

Chapter 4

Results

4.1 Aerosol Metrics

4.1.1 Statistical Analysis

We would expect that most of the aerosol parameters would correlate well with each other. For example, AI, AOD, and CLEARTOTAER should correlate extremely well with each other since these three parameters are looking at the aerosol concentration of the column. CLEARTOT should correlate well with these parameters as well since aerosols should be the biggest contribution to the vertically integrated attenuated backscatter since there should not be any other particles in the atmosphere that would have a large extinction cross-section. CLEARVIAB,

CLEARAERVIAB, CLEARLOW, CLEARLOWAER, VIAB, and AERVIAB may not correlate as well given the fact that these parameters will not integrate through the entire atmosphere and may miss aerosol layers. However, the four elevated calculations should correlate well in areas where there is minimal aerosol in the lowest one kilometer and CLEARLOW and CLEARLOWAER should correlate well when there is not an aerosol layer above one kilometer. As we have already seen, and will be shown quantitatively below, the correlation between the aerosol parameters, in many cases, is not as strong as one would expect. In order to isolate various aerosol effects and remove the confounding influence of meteorological properties, this study divided the data into 12 subsets. First, the data was previously divided into rainy and cloudy columns with the columns containing an aerosol layer identified. Next it was determined if the aerosol layer was above the cloud or touching the cloud. Again, a difference in aerosol base height and cloud top height of 250 m is the point at which this study divides the aerosol layers between touching and being above the cloud. At this point, there are four subsets within the data. Within each subset the top, middle, and bottom 10% of all liquid water path values were determined. LWP was calculated using equation 3.12. In the following figures these 12 subsets will be identified as: rain, above, top (RAT); rain, above, middle (RAM); rain, above, bottom (RAB); rain, touch, top (RTT); rain, touch, middle (RTM); rain, touch, bottom (RTB); cloud, above, top (CAT); cloud, above, middle (CAM); cloud, above, bottom (CAB); cloud touch top (CTT); cloud, touch,

middle (CTM); and cloud, touch, bottom (CTB). For each set of parameters a linear fit was calculated. Unless otherwise noted, all correlations shown below are statistically significant at or above 0.95.

The first set of correlations that will be shown is AI vs. CLEAERAERVIAB (Figure 4.1). This is a case where the correlations are moderately high. While

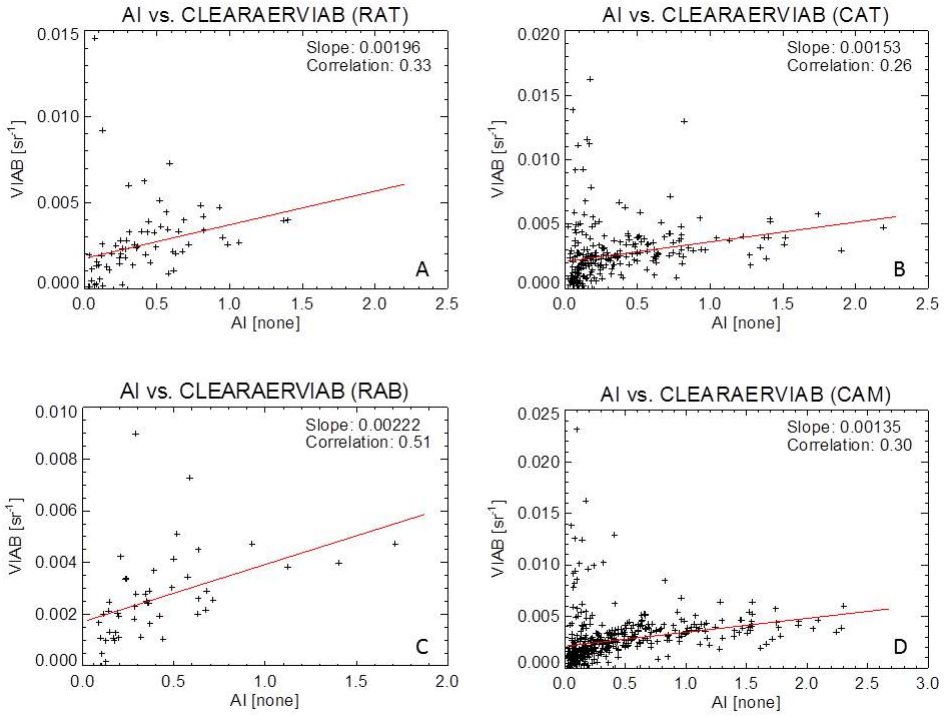

FIGURE 4.1: AI vs. CLEARAERVIAB for RAT (A), CAT (B), RAB (C), and CAM (D).

this combination of aerosol parameters does not have the highest correlations (AI vs. AERVIAB has the highest) this combination of aerosol metrics has a fairly consistent trend between the parameters as evidenced by the slope of the linear fit. The fact that AI vs. CLEARAERVIAB has such a consistent set of correlations and

slopes suggests that AI may be more representative of elevated aerosol layers than boundary layer aerosol layers. This point is further supported by the fact that the correlation between AI and AERVIAB is 0.46 (RAT), 0.30 (RAB), 0.44 (CAT), and 0.58 (CAM). Interestingly, AOD vs. CLEARTOTAER is one of the combinations that has poor correlations, especially in terms of consistency between subsets of the data. Out of the 12 categories, only two have statistically significant correlations, CAM (-0.09) and CAB (-0.1). Further supporting the fact that AI may not be representative of the boundary layer aerosol layer is that the correlations between AI and CLEARLOWAER are moderate and negative (Figure 4.2). Not only are

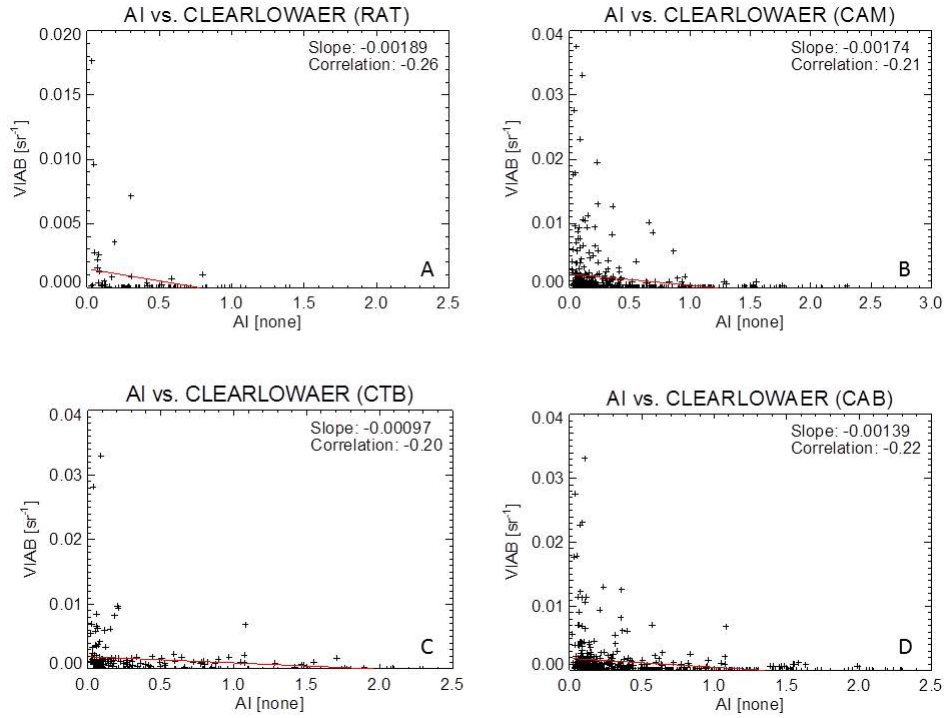

FIGURE 4.2: AI vs. CLEARLOWAER for RAT (A), CAM (B), CTB (C), and CAB (D).

the correlations negative, they are consistent as well. In these cases the slope between the parameters is consistent as well. While an argument could be made that CLEARLOW and CLEARLOWAER could have a negative slope, it is less clear that this argument can be made for CLEARTOT or CLEARTOTAER. Looking at figure 3.1, however, one notices that low aerosol appears to account for a majority of the total aerosol concentration during the months of January through March and October through December while the elevated aerosol contribution starts to become significant for the months of June through September when it surpasses the low aerosol contribution. Given this, it seems more plausible that there could be a negative correlation between AOD and CLEARTOTAER. It is interesting to note that elevated aerosol becomes the significant contribution to total aerosol during the biomass burning months.

Another way to look at the data is to try and determine if the trends within any of the subsets are robust. Looking at the trends in CTT for various aerosol parameter combinations (Figure 4.3), we see that this is a case where the correlation between the aerosol parameters is consistently positive and quite strong for AI and AOD vs. AERVIAB. Additionally, the slopes of the linear fit are similar to one another, especially for AI and AOD vs. AERVIAB and AI and AOD vs. CLEARAERVIAB. It is promising to see that the stronger correlations correspond with the steeper slopes. With that being said, the fact remains that there is a wide spread in the correlations within this subset of the data. Unfortunately, as was the case when

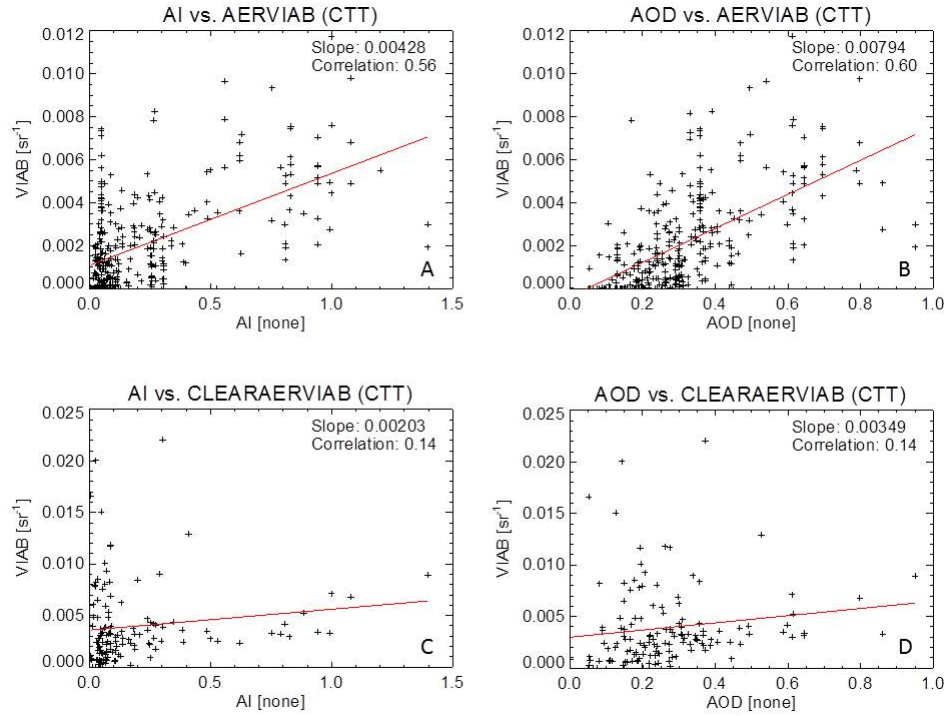

FIGURE 4.3: Cloud, Touch, Top for AI vs.AERVIAB (A), AOD vs. AERVIAB (B), AI vs. CLEARAERVIAB (C), and AOD vs. CLEARAERVIAB (D).

looking at aerosol parameter combinations, there are also inconsistent correlations within a subset of the data as well (Figure 4.4). In this case AI vs. AERVIAB (RAM) and AOD vs. CLEARAERVIAB (RAM) have a positive correlation while AOD vs. CLEARTOT (RAM) and AOD vs. CLEARLOWAER (RAM) have a negative correlation. The one promising aspect of the figure though is that is that we would not necessarily expect CLEARLOWAER to have as strong of a correlation with AI or AOD. With that being said, it is unclear whether this relationship should exhibit a negative correlation. In addition, there is a negative correlation between AOD and CLEARTOT. However, even if the negative correlations are

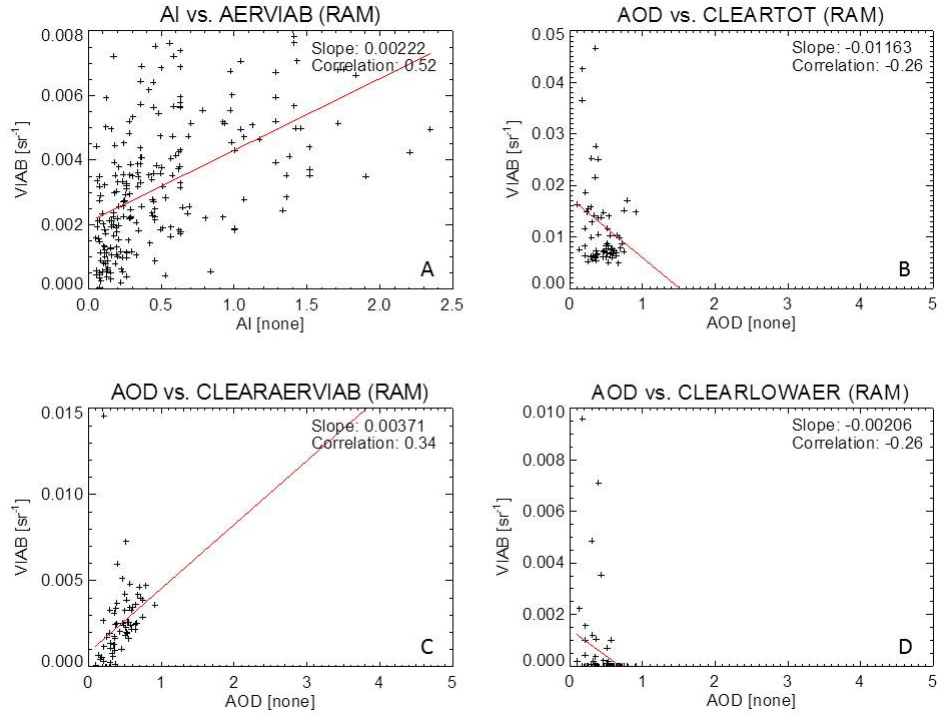

FIGURE 4.4: Rain, Above, Middle for AI vs. AERVIAB (A), AOD vs. CLEARTOT (B), AOD vs. CLEARAERVIAB (C), and AOD vs. CLEARLOWAER (D).

thrown out, assuming negative correlations are not physical, the correlation between the aerosol parameters within the CTT subset is weak and varied with the strongest correlation being 0.52 from the AI vs. AERVIAB combination and the weakest positive correlation being 0.15 from the the AOD vs.VIAB combination (not shown). This is a large difference when some of the correlations are not strong to begin with.

While the correlation between the various aerosol parameters are not great there is some hope that the aerosol metrics presented may be able to pick out a signal relating to the aerosol indirect and semi-direct effects. There are a number of

combinations that show promise, AI vs. AERVIAB and CLEARVIAB as well as AOD vs. AERVIAB and CLEARAERVIAB.

It is interesting to note that in cloudy columns the only combinations that have a negative correlation integrate through the lowest 1 km. The same can be said for rainy columns, with CLEARVIAB also having a negative correlation with AI for the RAT subset. There are a number of possible explanations for how a negative correlation can make physical sense. First, it is plausible that either MODIS does a better job with elevated aerosol layers or that CALIOP cannot accurately see aerosols in the lowest one kilometer. Second, it is possible that the aerosol layers in the lowest one kilometer, while significant, are optically thin and below the detection limit of MODIS.

4.1.2 Case Studies

Two case studies are presented below. For each case study a map of the region is shown with the aerosol concentration plotted on a map with a line overlaid indicating the satellite track, a profile of the CALIOP derived aerosol parameter plotted versus latitude and CALIOP backscatter and vertical feature mask profiles for that case. The profile of the CALIOP derived aerosol parameter will calculate the parameter for that column specifically, it will not be the 1°x1° average. The columns identified as rainy, cloudy, and clear will be identified. The first case

study consists of two aerosol parameters that have a strong correlation, AI and CLEARAERVIAB for August 7, 2010. The second case study consists of two aerosol parameters that have a weak correlation, AI and CLEARLOWAER for November 16, 2007.

4.1.2.1 Case Study 1

Shown in figure 4.5 is the CALIOP 1064 nm attenuated backscatter for August 7,

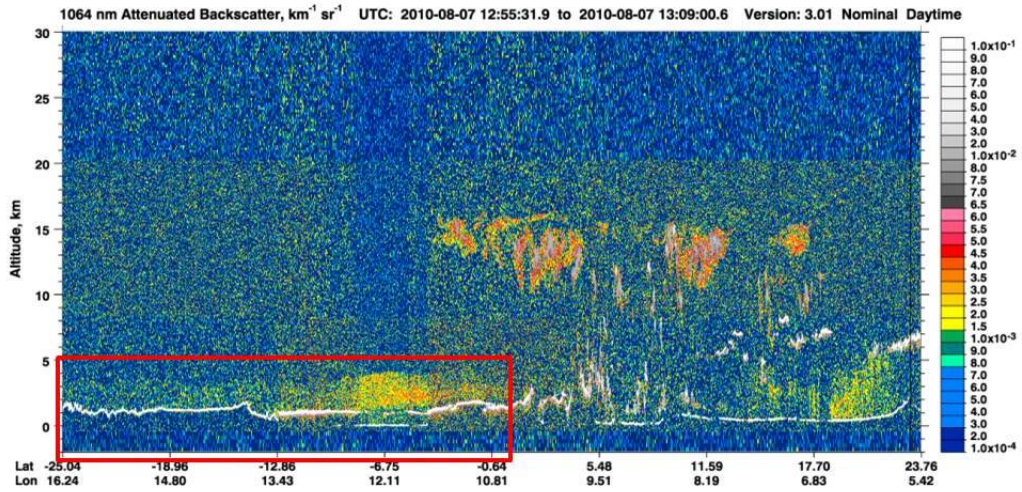

FIGURE 4.5: CALIOP 1064 Attenuated Backscatter for August 7, 2010 with the area of interest outlined in red.

2010 with the area of interest outlined in red. The left side of the figure, left of latitude -12.86° N, the satellite track is over land. Over the ocean we see a fairly persistent stratocumulus cloud layer, except for a region centered around -6.75° N. Centered over the same region there appears to be a fairly thick aerosol layer that extends over the cloud layer. From figure 4.6 we see that the aerosol layer, at

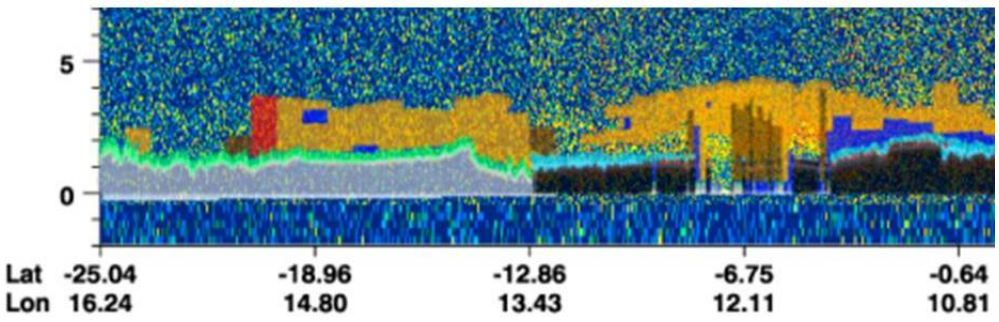

FIGURE 4.6: CALIOP VFM overlying 1064 Total Attenuated Backscatter for August 7, 2010 for the area of interest. Dark Blue-Clear Sky, Light Blue-Cloud, Orange-Aerosol, Green-Surface, Grey-Subsurface, Black-Totally Attenuated, Red-Cloud Low/No Confidence, Brown-Aerosol Low/No Confidence

least in terms of the scene classification algorithm, appears to be above the cloud layer in most, if not all, locations. From this figure it appears that the vertical feature mask is missing the bottom portion of the aerosol layer. This appears most obvious in the cloud free region left of the area identified as aerosol low/no confidence (brown). If CALIOP systematically misses the bottom of the aerosol layers, like it does in this case, this could have implications for the aerosol metrics that only integrate through aerosol layers.

Quantifying the aerosol concentration (Figure 4.7) we see that the aerosol concentration increases as one goes north for both CLEARAERVIAB and AI. In this case at least, CLEARAERVIAB appears to have a larger gradient in aerosol concentration than AI. From the MODIS AI data we can see that most of the study area is characterized by low background aerosol concentrations with pockets of enhanced aerosol concentrations. Looking at the profile of AERVIAB, there is clearly

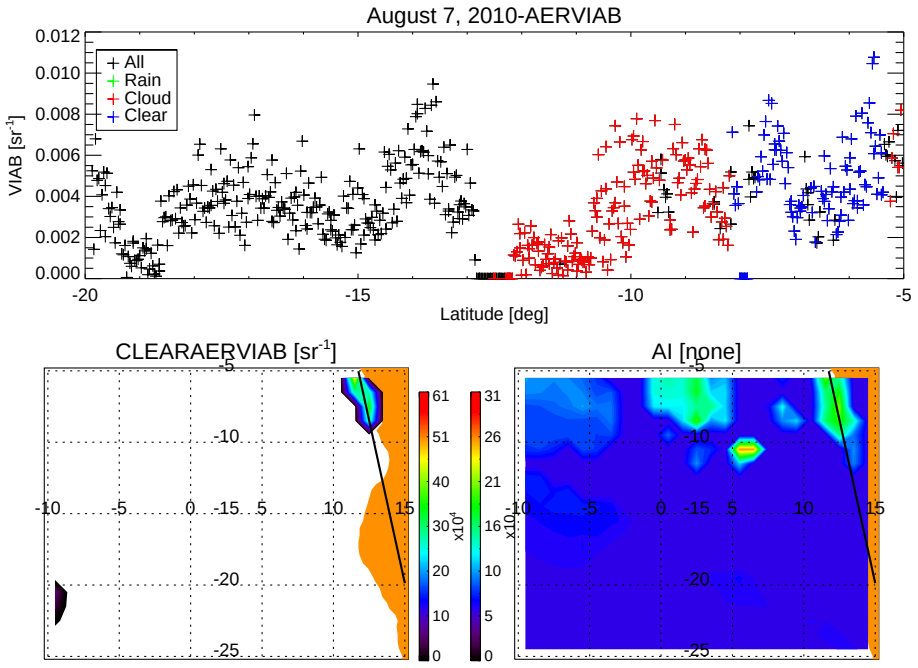

FIGURE 4.7: Map of aerosol concentration for August 7, 2010. Profile of AERVIAB (Top), map of CLEARAERVIAB (Bottom Left), map of AI (Bottom Right)

an increasing trend in aerosol concentration as the satellite moves north over the ocean. Over land there appears to be more of a constant aerosol concentration. It is important to note that from about -12° to about -8° N latitude the columns are identified as cloudy only and from about -8° to -5° N the columns are identified mainly as clear. Recall that CLEARAERVIAB, the variable that we are using in this case study, calculates aerosol concentration solely under clear sky conditions. This is why the map of CLEARAERVIAB does not have data south of -8° N. As a consequence, none of the cloudy columns will have a valid aerosol concentration in this case as there is not a clear sky column within the 1°x1° grid cell necessary for a retrieval of aerosol concentration. Therefore, most of the cloud microphysical

data would not be used in this case. However, if AERVIAB was the aerosol parameter being used, all of the data could be used. This could explain why AERVIAB correlates even better with AI than CLEARAERVIAB.

4.1.2.2 Case Study 2

Shown in figure 4.8 is the CALIOP 1064 nm attenuated backscatter for November

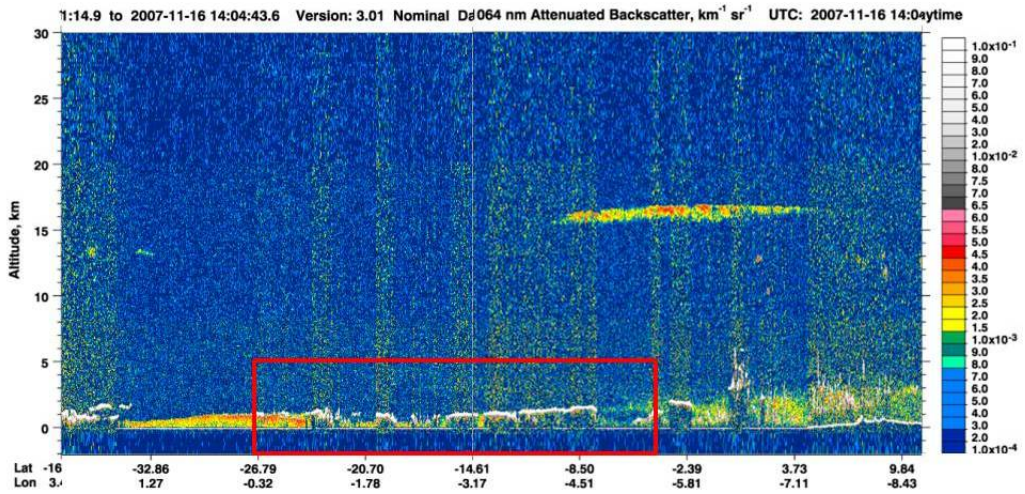

FIGURE 4.8: CALIOP 1064 Attenuated Backscatter for November 16, 2007 with the area of interest outlined in red.

16, 2007 with the area of interest outlined in red. Within the area of interest we see a broken stratocumulus cloud deck around one kilometer in altitude in the south and increasing to roughly two kilometers in altitude in the north. Except on the far right side of the area of interest, there does not appear to be an aerosol layer present above cloud top. An aerosol layer may be present within and below the cloud layer, however. Also, note the high clouds present on the right side of the

image, near -8° N. Areas with high altitude clouds are not included in the dataset. Looking at figure 4.9, the vertical feature mask agrees with the assessment of this

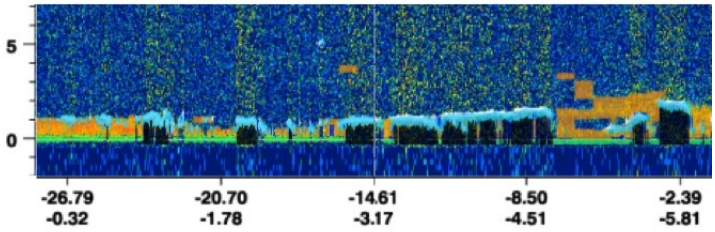

FIGURE 4.9: CALIOP VFM overlying 1064 Total Attenuated Backscatter for November 16, 2007 for the area of interest. Dark Blue-Clear Sky, Light Blue-Cloud, Orange-Aerosol, Green-Surface, Grey-Subsurface, Black-Totally Attenuated

scene. Most of the aerosol lies within the clear sky region on the right side of the area of interest. The vertical feature mask also identifies an aerosol layer below the cloud throughout most of the area of interest. Recall that this aerosol layer is ignored in the analysis, only aerosol layers above cloud top are identified as aerosol layers below cloud top cannot be reliably retrieved.

Quantifying the aerosol concentration (Figure 4.10) we immediately notice the very poor correlation between CLEARLOWAER and AI. CLEARLOWAER retrieves a high aerosol concentration to the south of -15° N while the AI data is fairly consistent along the satellite overpass track. AI also identifies a much more widespread aerosol layer, both on and off the satellite overpass track. In this case CALIOP must not be correctly identifying the aerosol layer as there are a lot of clear sky pixels identified in the satellite overpass, as seen in the top portion of figure 4.10. There is also the possibility that MODIS AI is too high, especially if the cloud

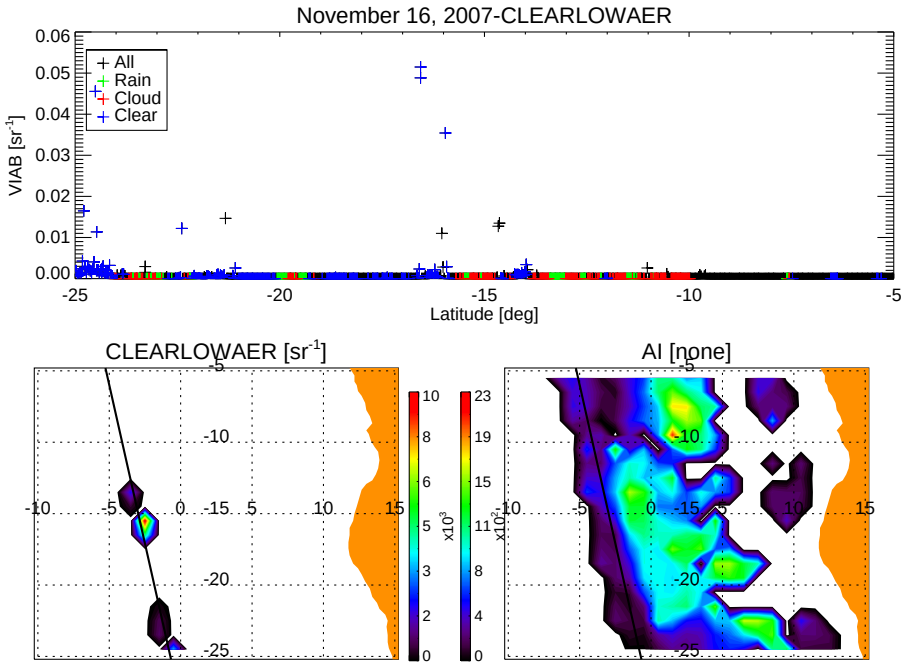

FIGURE 4.10: Map of aerosol concentration for November 16, 2007. Profile of AERVIAB (Top), map of CLEARTOTAER (Bottom Left), map of AOD (Bottom Right)

field is very heterogeneous in this area as MODIS would then suffer from 3-D cloud effects and cloud contamination, as mentioned previously.

4.2 Cloud Parameters

Even with the challenges presented above in regard to the correlation between the various aerosol parameters, there does appear to be an aerosol impact on cloud micro- and macro- physics. This section will look at the aerosol impact on three

parameters: cloud droplet number concentration, effective radius, and the probability of precipitation.

4.2.1 Cloud Droplet Number Concentration

Shown in figure 4.11 is CDNC plotted against one of the aerosol parameters. The

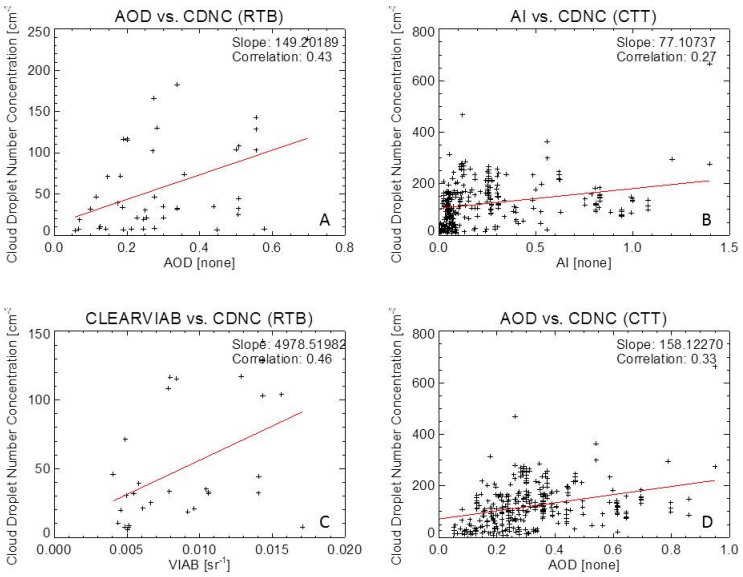

FIGURE 4.11: Cloud Droplet Number Concentration. AOD vs. CDNC (RTB)(A), AI vs. CDNC (CTT)(B), CLEARVIAB vs. CDNC (RTB)(C), AOD vs. CDNC (CTT)(D)

left two figures, figures A and C, have much higher correlations and steeper slopes than the two figures on the right. With that being said, the fact that all four figures show a consistent positive trend leads one to believe that an increase aerosol concentration does lead to an increase in CDNC. These data suggest, however, that we should be cautious when trying to quantify the exact relationship between aerosol

concentration and CDNC given that the slopes and correlations vary, even within this subset. Bearing that in mind, these plots still show results that are consistent with the first indirect aerosol effect. The remaining statistically significant aerosol vs. CDNC scatter plots can be found in Appendix A.

4.2.2 Effective Radius

Looking at figure 4.12 is the effective radius plotted against one of the aerosol pa-

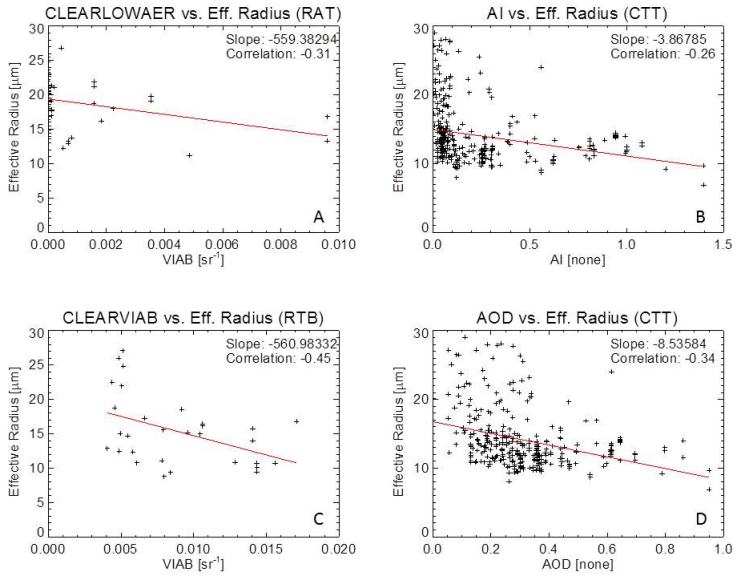

FIGURE 4.12: Effective Radius. CLEARLOWAER vs. Effective Radius (RAT)(A), AI vs. Effective Radius (CTT)(B), CLEARVIAB vs. Effective Radius (RTB)(C), AOD vs. Effective Radius (CTT)(D)

rameters. Three of the four figures (A, B, and D) have very similar correlations, with figure D having a much lower correlation than the other three. While three of

the correlations may be similar, there is still a significant variation in the correlation, as well as the slope, between the various combinations shown. As was the case with CDNC, we should be cautious when trying to quantify the exact relationship between aerosol concentration and effective radius given the spread in correlations and slopes. Again though, these plots point to the fact that an increase in aerosol concentration leads to a decrease in effective radius, results consistent with the first indirect aerosol effect. The remaining statistically significant aerosol vs. effective radius scatter plots can be found in Appendix A.

4.2.3 Probability of Precipitation

Shown in figure 4.13 is the probability of precipitation (PoP) for four different

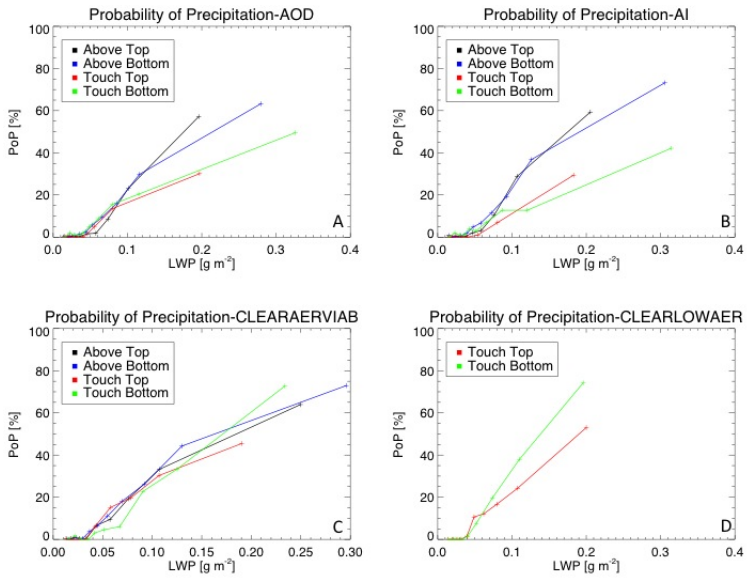

FIGURE 4.13: Probability of Precipitation. AOD (A), AI (B), CLEARAERVIAB (C), CLEARLOWAER(D)

aerosol metrics. These plots are different from the previous plots shown. The x-axis is now LWP, not aerosol concentration. The top and bottom, in this case then, represent the top and bottom 20% aerosol concentration values for whatever aerosol metric is being used. The top two figures, AI and AOD, show an increase in PoP with an increase in aerosol above the cloud, especially at the higher liquid water path values. An increase in aerosol above the cloud layer would increase the temperature of the atmospheric layer. This would increase the strength of the inversion capping the stratocumulus cloud layer. This would then further limit cloud growth. With constant LWP, a cloud should precipitate more efficiently if it is thinner as there is a greater chance of collision between the cloud droplets, increasing the efficiency of the collision-coalescence process. Note that this is not the semi-direct effect where liquid water path is expected to decrease in the presence of aerosols. CLEARAERVIAB shows an increase in PoP with decreasing aerosol concentration above the cloud. An explanation for this discrepancy was not found. AOD, CLEARAERVIAB, and especially CLEARLOWAER show a decrease in PoP with an increase in aerosol concentration when the aerosol layer is touching the cloud. This is consistent with the first and second indirect aerosol effects. CLEARLOWAER should be especially sensitive to this change as this is the aerosol layer that would get ingested into the cloud through updrafts, not just entrainment through turbulent mixing at cloud top, as is the case with the aerosol layers that are touching the cloud from above. Since all CCN do not become cloud

droplets, the ingestion of aerosol at cloud base would increase the amount of time that an aerosol has to become activated and form a cloud droplet. AI shows an increase in PoP with an increase in aerosol concentration touching the cloud. An explanation for the discrepancy between AI and the other three aerosol parameters shown has not been found. The PoP for the other six aerosol parameters are shown in Appendix B.

4.3 Challenges

Almost every result shown has had either varying correlations and slopes or contradictory results. In many cases an attempt was made to identify some of the challenges associated with that data and a possible explanation. This section will highlight some of these challenges, as well as many new ones, that have been documented in the literature that could have an affect on the results shown.

Haywood et al. (2004) found that aerosols located above cloud layers may affect the COD and effective radius retrievals from MODIS. Using the default MODIS channel combination of 0.86 μm and 2.1 μm, COD is more affected by aerosol overlying a cloud than effective radius. In cases with an overlying aerosol layer the COD will be underestimated, the amount determined by the AOD of the aerosol layer. An error in COD could affect the results of this study in multiple ways. First, COD is used in scene classification. If COD is underestimated this study could be

throwing out legitimate rainy and cloudy cases that did not meet this threshold. Second, COD is then used as input into the equations for LWP and CDNC. LWP is also a variable in the equation for CDNC. Therefore, underestimating COD could lead to more data being thrown out, a decrease in LWP, and an increase in CDNC. The quantitative effects this could have are beyond the scope of this study.

Breon and Doutriaux-Boucher (2005) found that the MODIS effective radius retrieval is sensitive to cloud heterogeneity. A decrease in cloud fraction (increase in cloud heterogeneity) leads to an overestimation of the effective radius. Given the heterogeneity of the stratocumulus cloud layer in this area, this most likely has an have an affect on the effective radius in this study. In turn, this could lead to an overestimation the liquid water path calculation and CDNC calculation.

Kacenelenbogen et al. (2014) found that CALIOP, when compared with High Spectral Resolution Lidar from NASA Langley, detects only 23% of AAC cases. The study found that the underestimation of AAC is the result of extremely thin aerosol layers ($\tau > 0.02$) that fall below the detection limit of CALIOP. Another explanation for the underestimation of AAC by CALIOP is incorrect aerosol type classification (Omar et al. 2009). This could be caused by low signal-to-noise ratio or the use of loading-dependent lidar measurements that are only loosely related to aerosol type. If the same statistics hold for the southeastern Atlantic Ocean, this could explain the low fraction of rainy (25%) and cloudy (28%) that have an aerosol layer

above cloud top in this study. Better detection of AAC layer would lead to more accurate integrated backscatter values when integrating through aerosol layers.

Another potential source of error between MODIS and CALIOP derived aerosol concentration is that in AOD retrievals MODIS assumes a value for aerosol absorption. However, Eck et al. (2013) found that this assumption leads to a single scatter albedo induced bias within the MODIS AOD retrieval as the study found a seasonal cycle in single scatter albedo in southwestern Africa. The single scatter albedo increases from 0.81 in July to 0.92 in November, which leads to a factor of 2 difference in optical depth as a result of absorption.

Winker et al. (2009) also lists possible sources of error in the calculation of CALIOP AOD. Possible sources of error include: instrument calibration and normalization errors, errors in cloud-aerosol discrimination, layer boundary detection, multiple scattering, and *a priori* lidar ratios. Tanre et al. (1997) had previously identified possible sources of error in the calculation of AOD from MODIS. The sources of error include: surface reflection, sensor calibration, contamination by glint, water-leaving radiance, and uncertainties involved in the lookup tables such as aerosol size distribution, refractive index, and single-scattering albedo. Depending on the situation where each type of error could occur, this could contribute to the low correlation between the MODIS derived and CALIOP derived aerosol concentrations. With regard to aerosol misclassification, Kim et al. (2013) found that the large difference in biomass burning AOD between MODIS and CALIOP is the result of

incorrect identification of aerosol layer base altitude. In that study it was shown that most CALIOP AOD does not extend into the marine boundary layer, leading to an underestimation of CALIOP AOD. Evidence of this was seen in Case Study 1 where the bottom of the aerosol layer did not appear to be identified by the CALIOP vertical feature mask.

Another possible challenge in assessing the affect of aerosols on clouds is the hygroscopicity of aerosols. As humidity increases aerosols tend to swell, the amount of swelling is dependent on the hygroscopic properties of the specific aerosol. Twohy et al. (2009) showed that an increase in relative humidity causes the aerosol particle to grow, subsequently causing the scattering cross-section to increase. In turn, this increases the apparent aerosol concentration retrieved from satellites. An increase in aerosol concentration with increasing cloud cover has been reported in many satellite-based studies (Ignatov et al. 2005; Kaufman et al. 2005; Koren et al. 2007; Loeb and Manalo-Smith 2005; Loeb and Schuster 2008; Matheson et al. 2006; Quaas et al. 2008; Sekiguchi et al. 2003). As a consequence, hygroscopic swelling of aerosols could play an important role in the results of this study.

Additionally, aerosol and cloud parameters may co-vary as a result of meteorological conditions. In some cases, changes in meteorological conditions may be greater than the aerosol induced changes (e.g. Petters et al. 2013). Another challenge noticed in this study is that clear-sky columns may not be spatially located near the clouds being studied. This was seen in Case Study 1 where there was a 4°

range of cloud columns identified without a single clear column identified. As a consequence, none of the cloud data could be used with the MODIS or CALIOP clear-sky derived aerosol parameters. North of -8° N there was a range of clear columns with very limited cloud columns in the area. In this case, most of the aerosol data would go unused as there was not a cloud nearby to assign to the aerosol concentration.

Chapter 5

Conclusions

This study has shown that the correlation between aerosol metrics varies greatly. The correlations between AI and CLEARAERVIAB (R: 0.14-0.51), AI and AERVIAB (R: 0.28-0.58), AOD and CLEARAERVIAB (R: 0.15-0.34), and AOD and AERVIAB (R: 0.11-0.6) are moderate while the correlations between AI and CLEARLOWAER (R: -0.27-(-0.18)) and AOD and CLEARLOWAER (R: -0.26-(-0.16)) are quite low. A number of possible explanations regarding the lack of a strong correlation were presented in detail in the previous section. There are multiple explanations regarding the low correlation between AI, AOD, and CLEARLOWAER. First, it is possible that CALIOP cannot accurately sense aerosols in the lowest one kilometer. While it is true that CPR aboard CloudSat has this issue there is no reason to believe this is the case with CALIOP, especially over the depth of one kilometer.

Second, MODIS may have trouble viewing aerosols in the lowest one kilometer. As MODIS is a passive instrument, this should not be a major issue. Lastly, aerosol layers in the lowest one kilometer can be extremely thin, potentially below the detection limit of MODIS. Of the three possibilities, this las option seems the most promising.

One other possible issue is that in AOD retrievals MODIS assumes a value for aerosol absorption. However, Eck et al. (2013) found that the single scatter albedo increases from 0.81 in July to 0.92 in November, which leads to a factor of 2 difference in optical depth as a result of absorption.

In many cases different aerosol metrics can give vastly different results, in some cases even the sign of the trend can change. This was the case when four combinations of aerosol metrics were shown for the subset RAM (Figure 4.4). In this case the correlation between the aerosol parameters ranged form $R = -0.26$ to $R = 0.52$. When such a large range is present, it is harder to trust the data. However, there is still a possibility that the trends are real as the negative correlations involve CLEARLOWAER and CLEARTOT. As just mentioned, there could be a physical explanation for the negative correlation. It is this type of result, however, that leads to some of the challenges one encounters when trying to assess the aerosol indirect and semi-direct effects.

Even with the challenges associated with this type of study there appears to be an

identifiable affect of aerosols on cloud micro- and macro- physics. As was shown, there is a positive correlation between aerosol concentration and CDNC and a negative correlation between aerosol concentration and effective radius. In both cases this result is consistent with the first aerosol indirect effect. Assuming LWP is held constant, which can be done as this study looked only at the top, middle, and bottom 10% of aerosols, not the entire aerosol range, an increase in aerosol concentration will lead to an increase in CDNC. Since LWP is constant, this increase in CDNC leads to a decrease in effective radius. This is exactly what was seen with the results presented in this study.

Through the probability of precipitation, the second aerosol indirect effect was studied. There is evidence to support the hypothesis that an increase in aerosol concentration will lead to a decrease in precipitation efficiency. This was seen by the fact that columns within the top 20% of aerosol concentration touching the cloud had a decrease in precipitation efficiency when compared to the columns in the bottom 20% of aerosol concentration. This is most evident in the PoP plot for CLEARLOWAER. While not necessarily representative of the biomass burning aerosols that were the focus of the study, this layer should have the largest impact on cloud formation. Aerosols within this layer would be injected into the cloud in the updraft, a much more efficient process than the turbulent mixing that would need to occur to mix aerosols layers above the cloud. In addition, aerosols injected from below will have a longer lifetime in the cloud and have a greater chance

of being activated and become CCN. There could also be an effect of aerosol on PoP when the aerosol layer is above cloud top, instead of touching cloud top. In this case it looks like there is an increase in PoP with an increase in aerosol concentration, especially at larger LWP values. The aerosol layers above the cloud should increase the temperature of that layer as a result of absorption. This should strengthen the inversion capping the stratocumulus cloud layer. The cloud would then precipitate more efficiently as the same LWP is confined to a smaller area, increasing the efficiency of the collision-coalescence process. As mentioned earlier, the analysis presented cannot diagnose the semi-direct effect as liquid water path should decrease in the presence of an absorbing aerosol layer above cloud top and this analysis is done with liquid water path held constant.

To study the effect of aerosol above clouds, future studies should subset the dataset further and divide the above cloud subset into multiple levels. For example, it seems unreasonable to think that an aerosol layer three kilometers above cloud top would have the same effect on cloud macro- and micro- physics as an aerosol layer only a kilometer above cloud top. In this study however, both sets of cases would have been combined into a single subset. Future studies should also include the CALIPSO Lidar Cloud and Aerosol Discrimination (CAD) score. Inclusion of the CAD score would be a further guarantee that clouds and aerosols are properly identified within the dataset.

Appendix A

Cloud Parameters

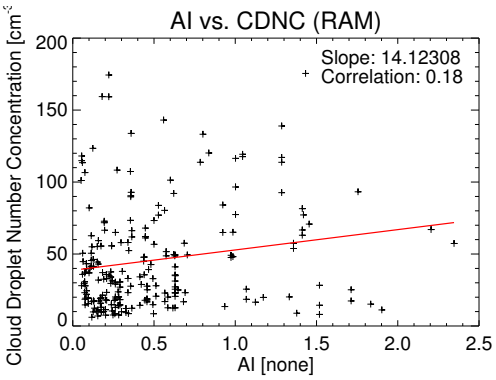

FIGURE A.1: CDNC: AI (RAM)

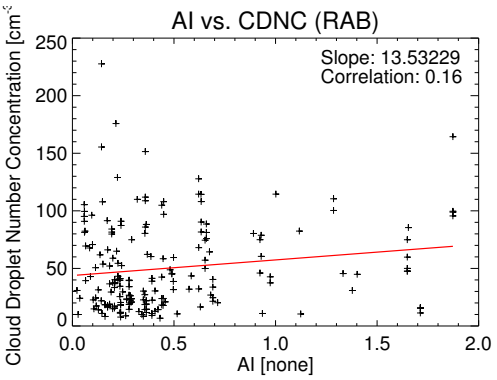

FIGURE A.2: CDNC: AI (RAB)

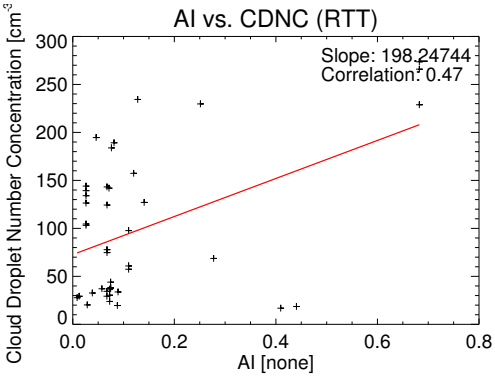

FIGURE A.3: CDNC: AI (RTT)

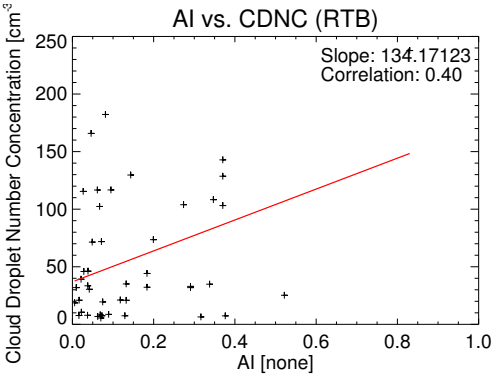

FIGURE A.4: CDNC: AI (RTB)

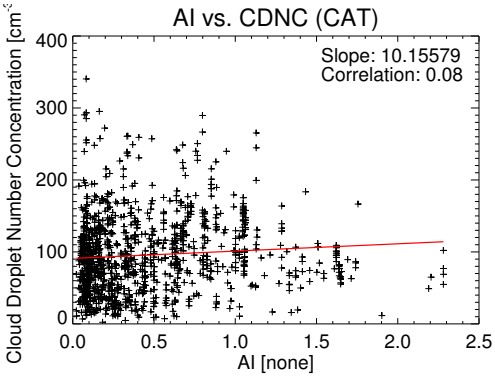

FIGURE A.5: CDNC: AI (CTT)

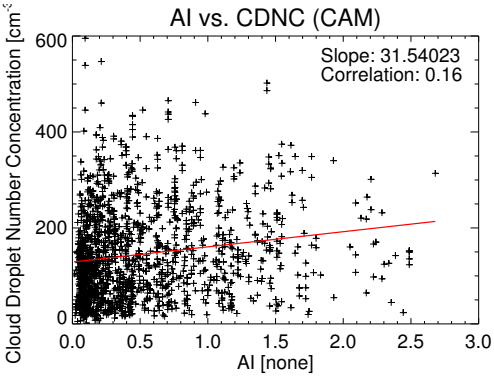

FIGURE A.6: CDNC: AI (CAM)

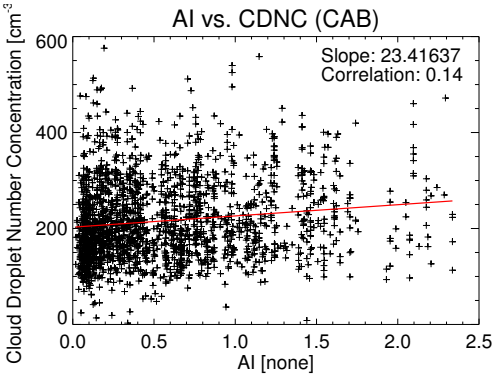

FIGURE A.7: CDNC: AI (CAB)

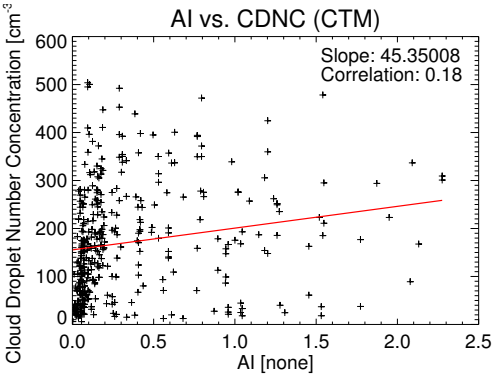

FIGURE A.8: CDNC: AI (CTM)

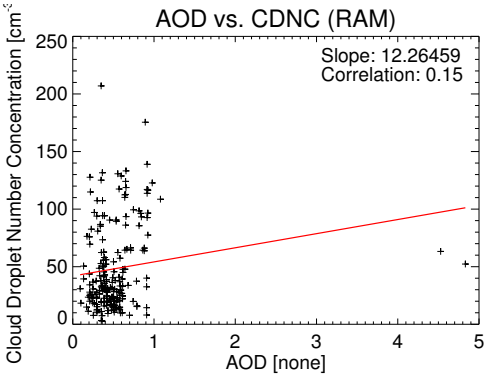

FIGURE A.9: CDNC: AOD (RAM)

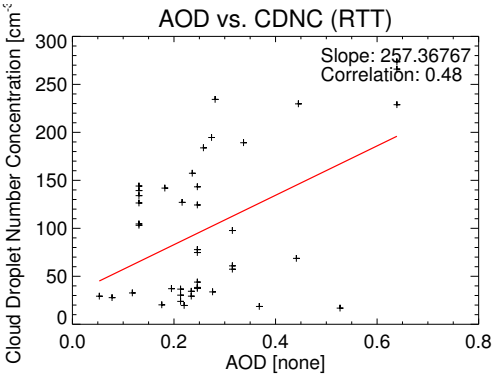

FIGURE A.10: CDNC: AOD (RTT)

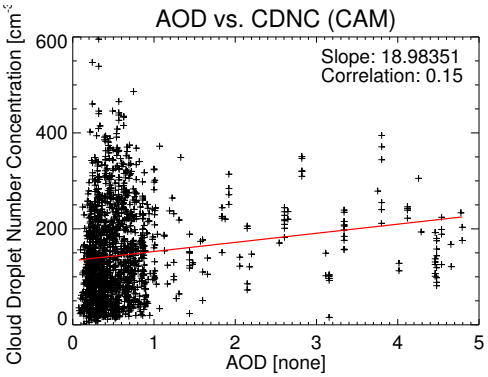

FIGURE A.11: CDNC: AOD (CAM)

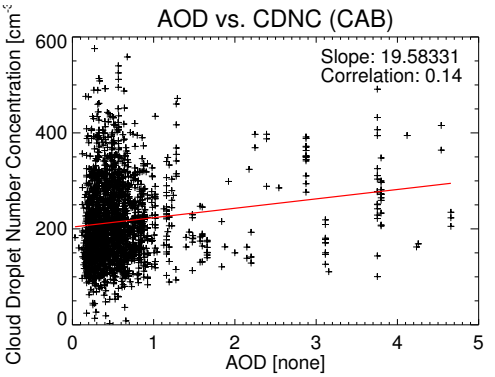

FIGURE A.12: CDNC: AOD (CAB)

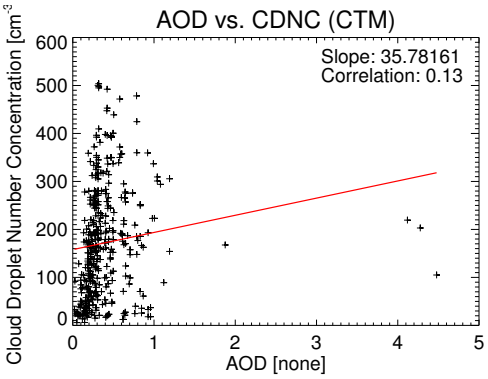

FIGURE A.13: CDNC: AOD (CTM)

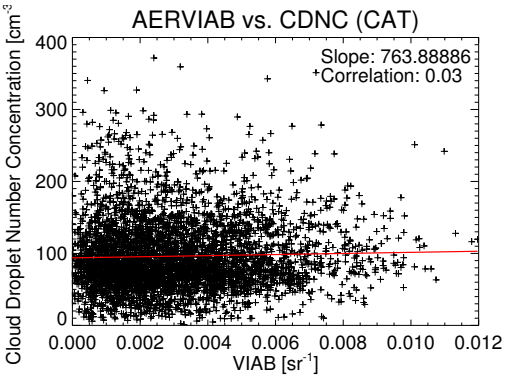

FIGURE A.14: CDNC: AERVIAB (CAT)

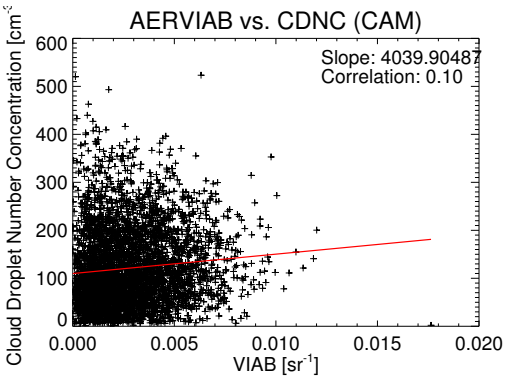

FIGURE A.15: CDNC: AERVIAB (CAM)

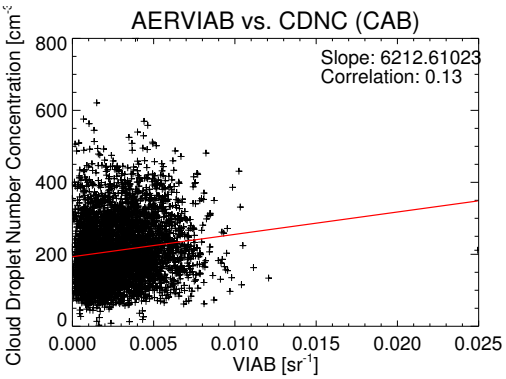

FIGURE A.16: CDNC: AERVIAB (CAB)

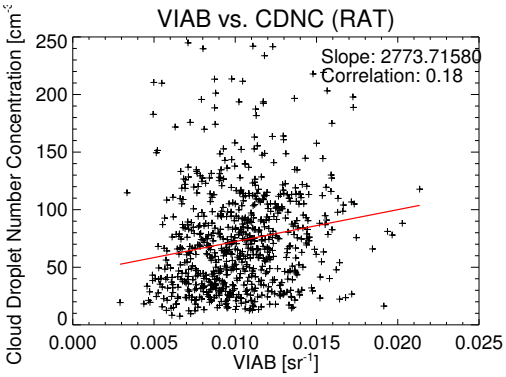

FIGURE A.17: CDNC: VIAB (RAT)

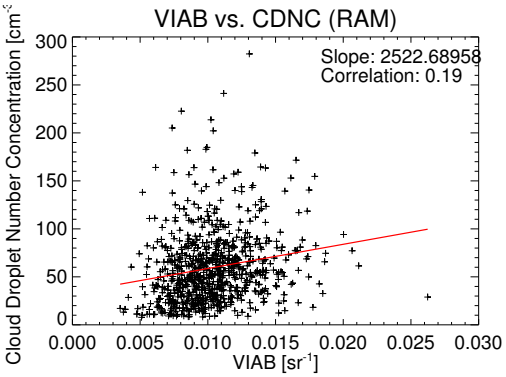

FIGURE A.18: CDNC: VIAB (RAM)

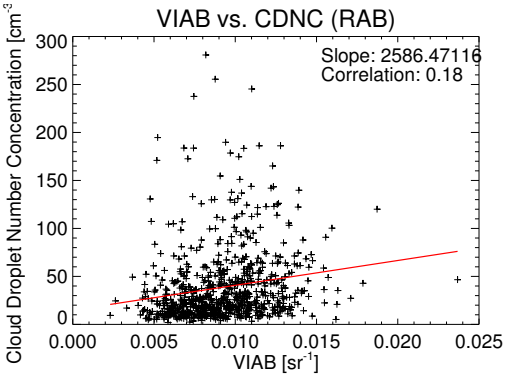

FIGURE A.19: CDNC: VIAB (RAB)

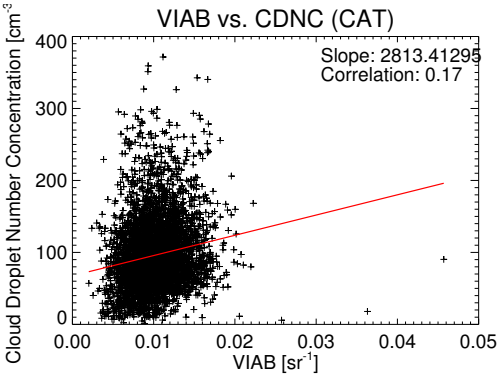

FIGURE A.20: CDNC: VIAB (CAT)

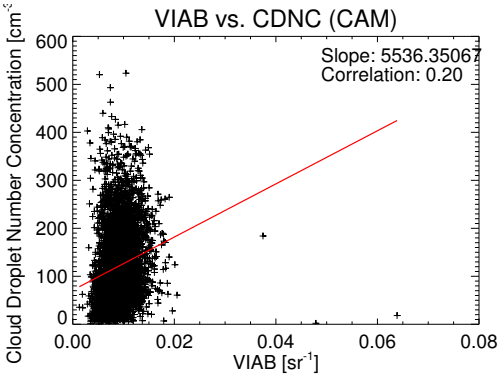

FIGURE A.21: CDNC: VIAB (CAM)

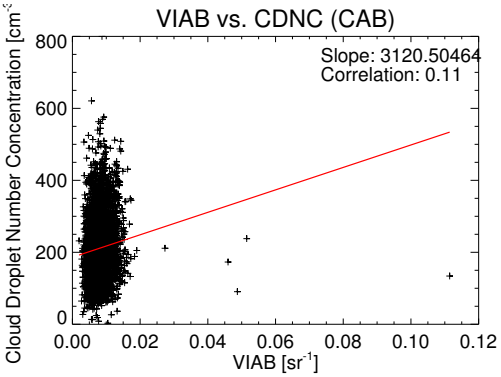

FIGURE A.22: CDNC: VIAB (CAB)

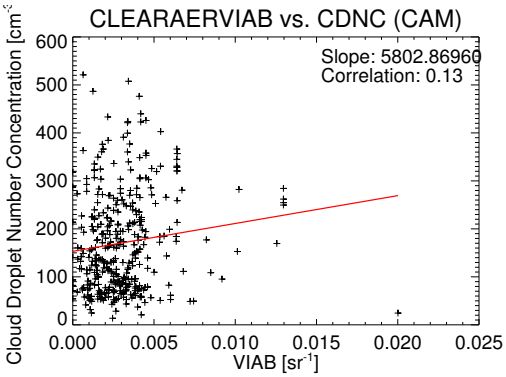

FIGURE A.23: CDNC: CLEAR-AERVIAB (CAM)

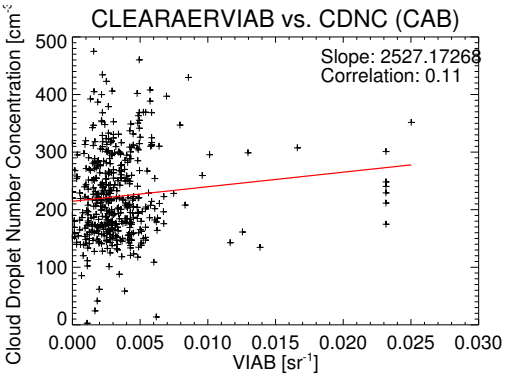

FIGURE A.24: CDNC: CLEAR-AERVIAB (CAB)

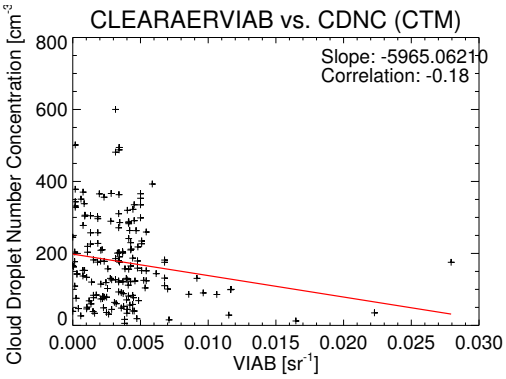

FIGURE A.25: CDNC: CLEAR-AERVIAB (CTM)

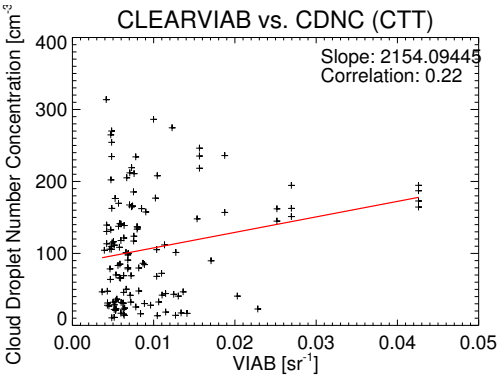

FIGURE A.26: CDNC: CLEARVIAB (CTT)

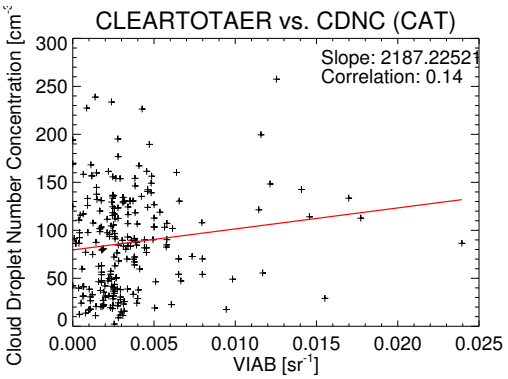

FIGURE A.27: CDNC: CLEARTOTAER (CAT)

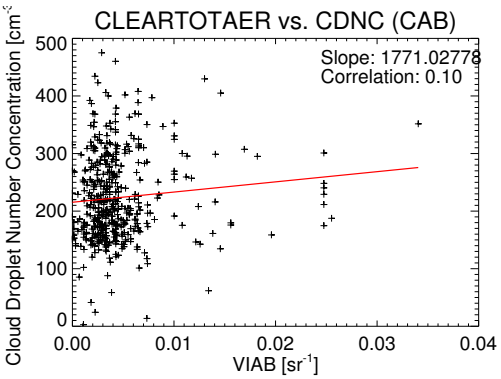

FIGURE A.28: CDNC: CLEARTOTAER (CAB)

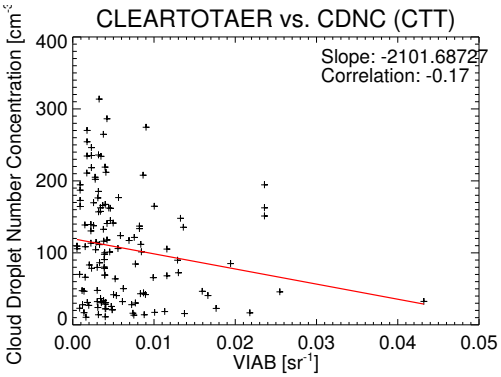

FIGURE A.29: CDNC: CLEARTOTAER (CTT)

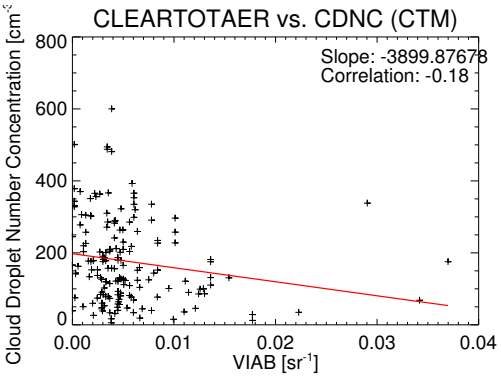

FIGURE A.30: CDNC: CLEARTOTAER (CTM)

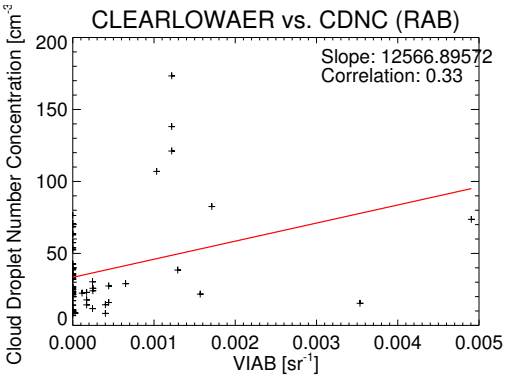

FIGURE A.31: CDNC: CLEARLOWAER (RAB)

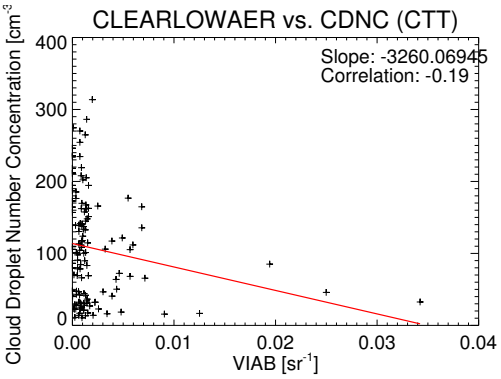

FIGURE A.32: CDNC: CLEARLOWAER (CTT)

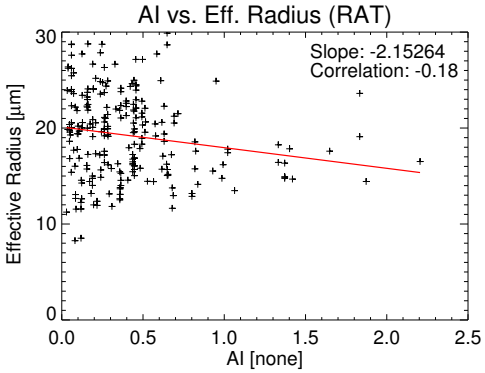

FIGURE A.33: Eff. Radius: AI (RAT)

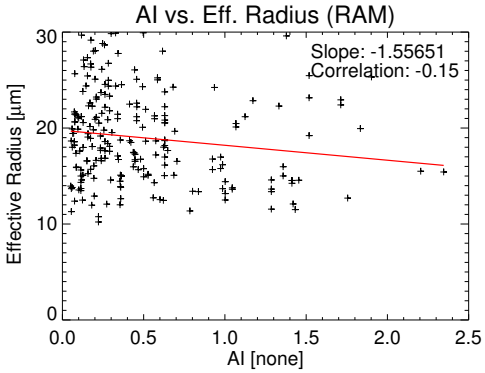

FIGURE A.34: Eff. Radius: AI (RAM)

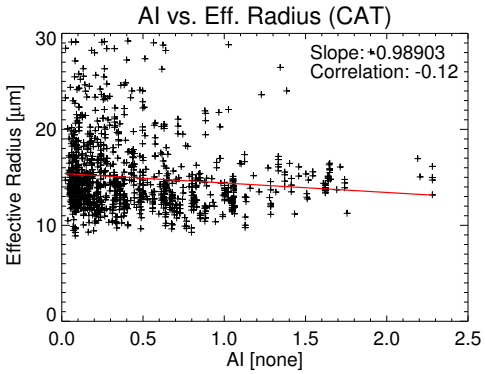

FIGURE A.35: Eff. Radius: AI (CAT)

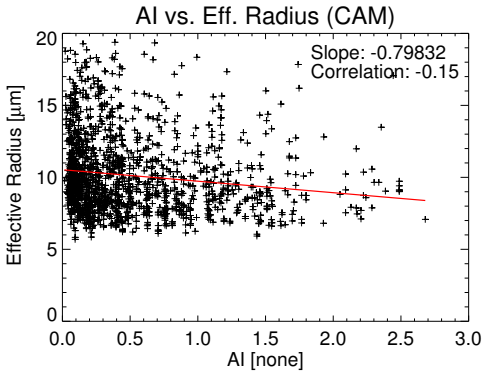

FIGURE A.36: Eff. Radius: AI (CAM)

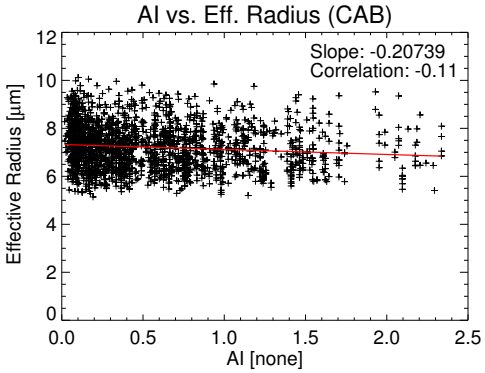

FIGURE A.37: Eff. Radius: AI (CAB)

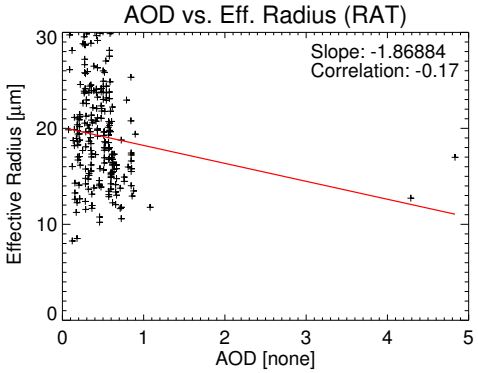

FIGURE A.38: Eff. Radius: AOD (RAT)

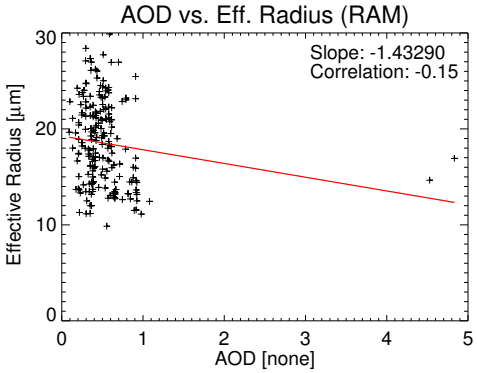

FIGURE A.39: Eff. Radius: AOD (RAM)

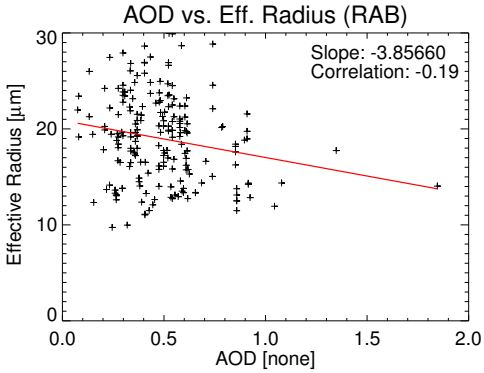

FIGURE A.40: Eff. Radius: AOD (RAB)

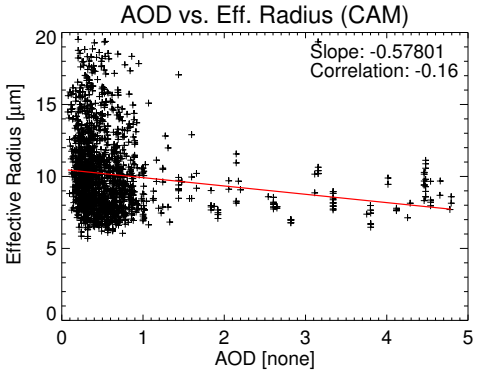

FIGURE A.41: Eff. Radius: AOD (CAM)

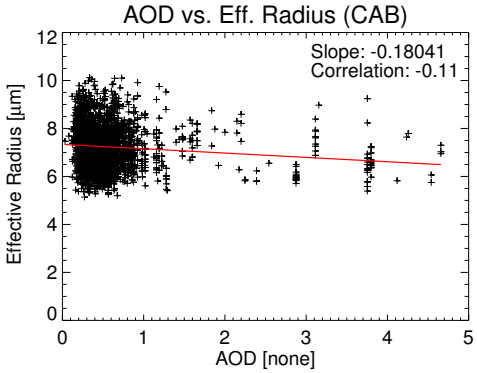

FIGURE A.42: Eff. Radius: AOD (CAB)

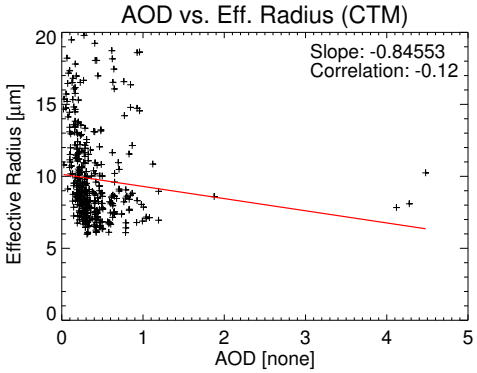

FIGURE A.43: Eff. Radius: AOD (CTM)

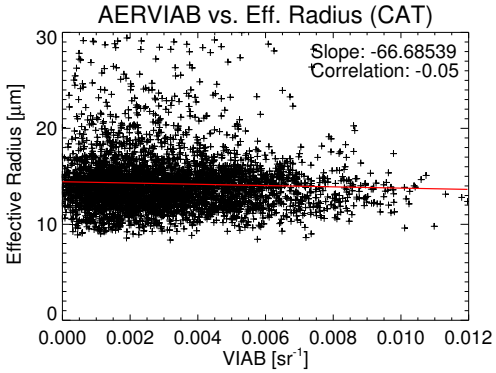

FIGURE A.44: Eff. Radius: AERVIAB (CAT)

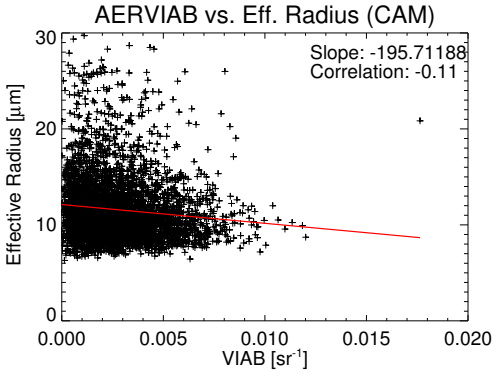

FIGURE A.45: Eff. Radius: AERVIAB (CAM)

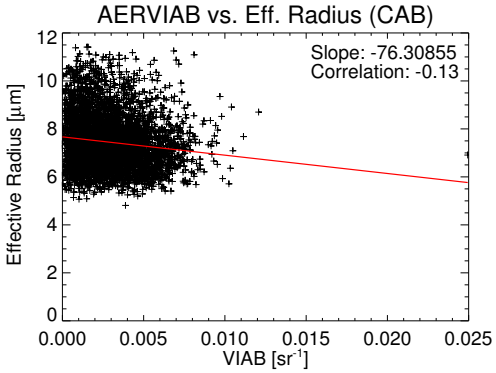

FIGURE A.46: Eff. Radius: AERVIAB (CAB)

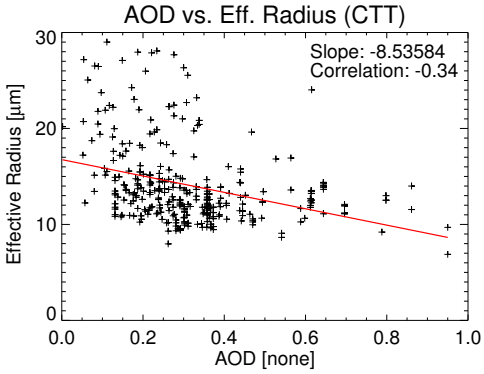

FIGURE A.47: Eff. Radius: AOD (CTT)

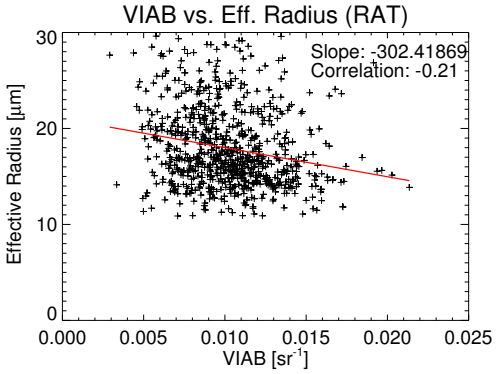

FIGURE A.48: Eff. Radius: VIAB (RAT)

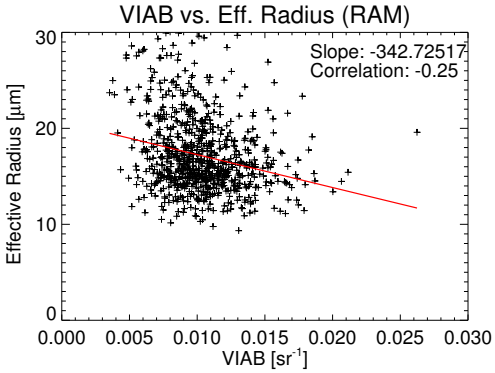

FIGURE A.49: Eff. Radius: VIAB (RAM)

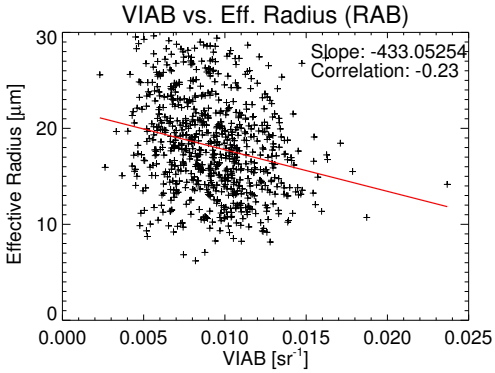

FIGURE A.50: Eff. Radius: VIAB (RAB)

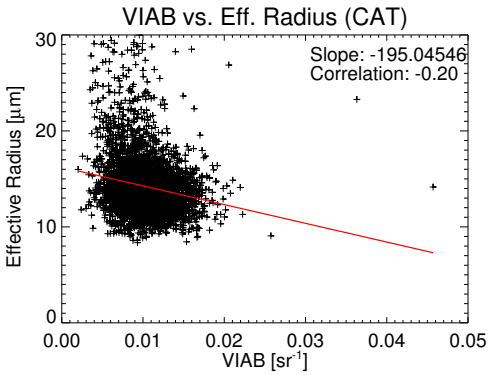

FIGURE A.51: Eff. Radius: VIAB (CAT)

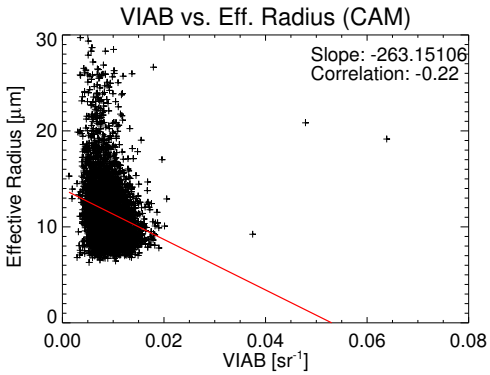

FIGURE A.52: Eff. Radius: VIAB (CAM)

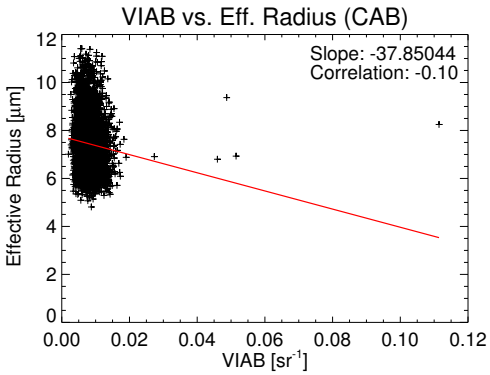

FIGURE A.53: Eff. Radius: VIAB (CAB)

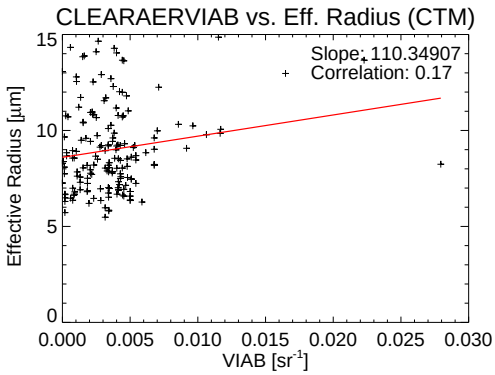

FIGURE A.54: Eff. Radius: CLEARAERVIAB (CTM)

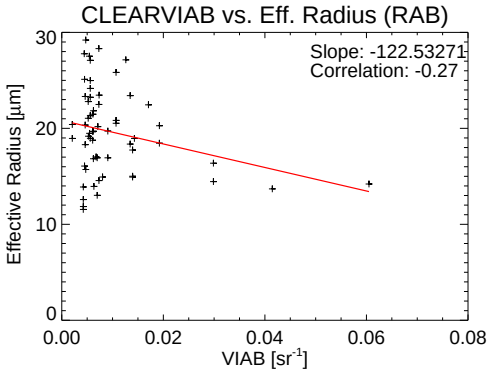

FIGURE A.55: Eff. Radius: CLEARVIAB (RAB)

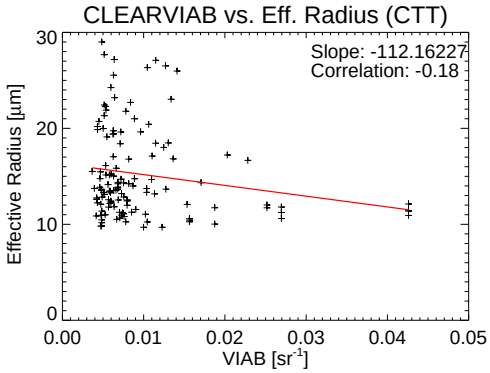

FIGURE A.56: Eff. Radius: CLEARVIAB (CTT)

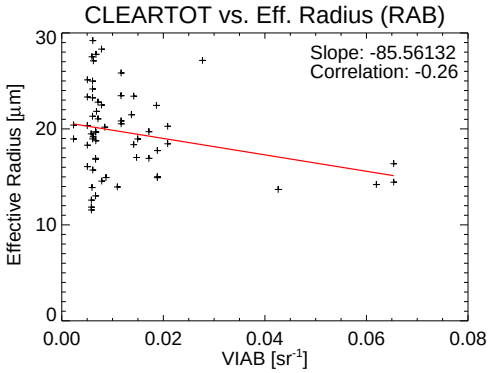

FIGURE A.57: Eff. Radius: CLEARTOT (RAB)

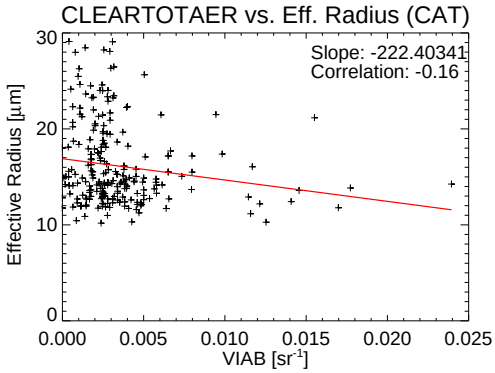

FIGURE A.58: Eff. Radius: CLEARTOTAER (CAT)

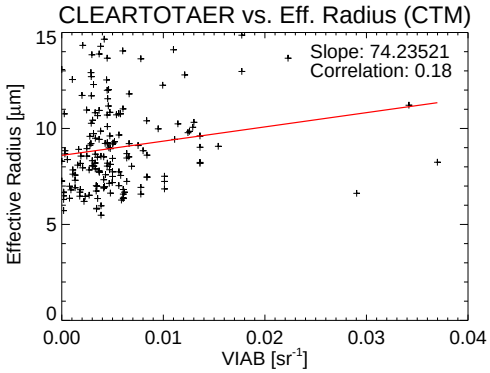

FIGURE A.59: Eff. Radius: CLEARTOTAER (CTM)

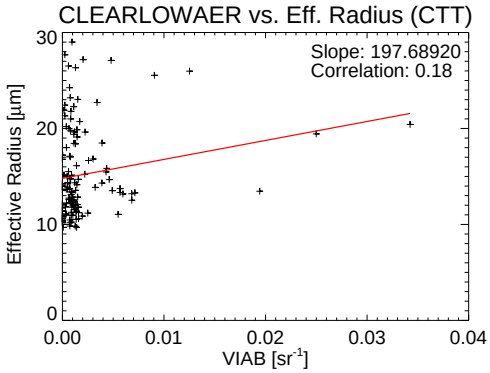

FIGURE A.60: Eff. Radius: CLEARLOWAER (CTT)

Appendix B

Probability of Precipitation

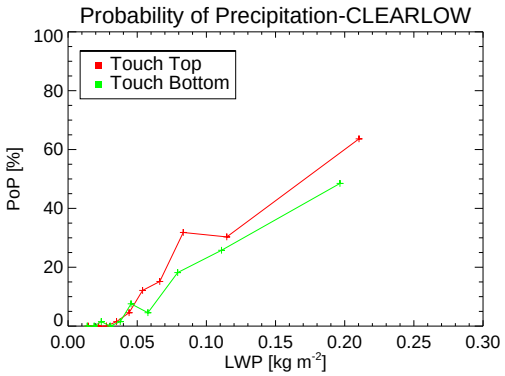

FIGURE B.1: Probability of Precipitation: CLEARLOW

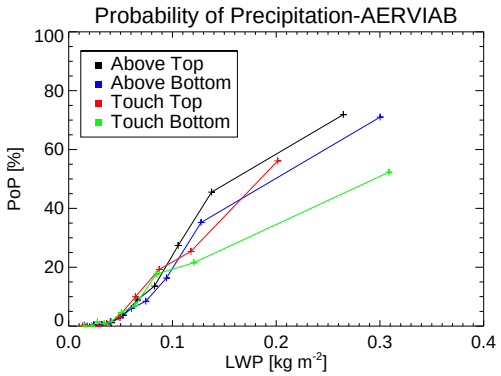

FIGURE B.2: Probability of Precipitation: AERVIAB

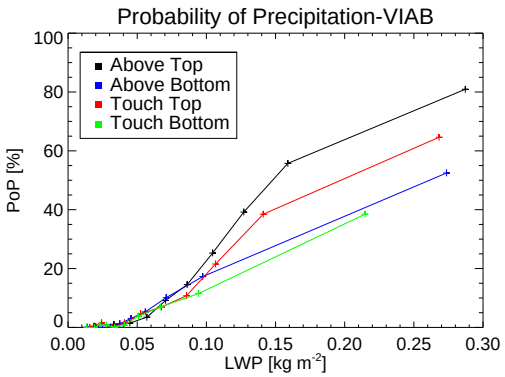

FIGURE B.3: Probability of Precipitation: VIAB

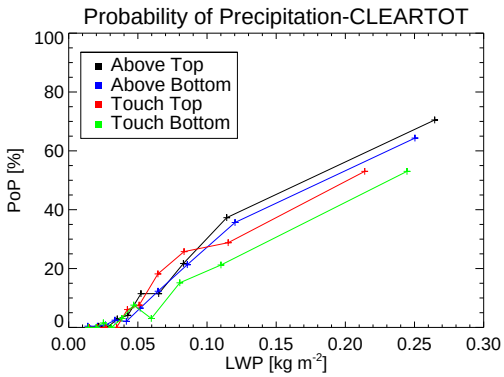

FIGURE B.4: Probability of Precipitation: CLEARTOT

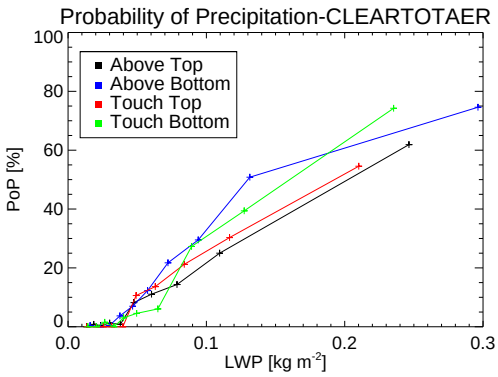

FIGURE B.5: Probability of Precipitation: CLEARTOTAER

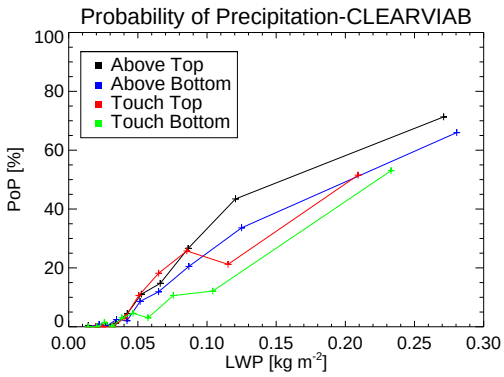

FIGURE B.6: Probability of Precipitation: CLEARVIAB

Bibliography

Ackerman, A., O. Toon, D. Stevens, A. Heymsfield, V. Ramanathan, and E. Welton, 2000: Reduction of tropical cloudiness by soot. *SCIENCE*, **288 (5468)**, 1042–1047, doi:{10.1126/science.288.5468.1042}.

Albrecht, B., 1989: Aerosols, cloud microphysics, and fractional cloudiness. *SCIENCE*, **245 (4923)**, 1227–1230, doi:{10.1126/science.245.4923.1227}.

Bennartz, R., 2007: Global assessment of marine boundary layer cloud droplet number concentration from satellite. *Journal of Geophysical Research-Atmospheres*, **112 (D2)**, doi:ArtnD02201Doi10.1029/2006jd007547, URL <GotoISI>://000243849400004.

Bennartz, R., J. Fan, J. Rausch, L. R. Leung, and A. K. Heidinger, 2011: Pollution from China increases cloud droplet number, suppresses rain over the East China Sea. *GEOPHYSICAL RESEARCH LETTERS*, **38**, doi:{10.1029/2011GL047235}.

Breon, F. M. and M. Doutriaux-Boucher, 2005: A comparison of cloud droplet radii measured from space. *Geoscience and Remote Sensing, IEEE Transactions on*, **43 (8)**, 1796–1805.

Chin, H. N. S., D. J. Rodriguez, R. T. Cederwall, C. C. Chuang, A. S. Grossman, J. J. Yio, Q. Fu, and M. A. Miller, 2000: A microphysical retrieval scheme for continental low-level stratiform clouds: Impacts of the subadiabatic character on microphysical properties and radiation budgets. *Monthly Weather Review*, **128 (7)**, 2511–2527, URL <GotoISI>://000166058500008.

Costantino, L. and F. M. Breon, 2013: Aerosol indirect effect on warm clouds over South-East Atlantic, from co-located MODIS and CALIPSO observations. *ATMOSPHERIC CHEMISTRY AND PHYSICS*, **13 (1)**, 69–88, doi:{10.5194/acp-13-69-2013}.

Cotton, W. R., G. J. Tripoli, R. M. Rauber, and E. A. Mulvihill, 1986: Numerical-Simulation of the Effects of Varying Ice Crystal Nucleation Rates and Aggregation Processes on Orographic Snowfall. *Journal of Climate and Applied Meteorology*, **25 (11)**, 1658–1680, URL <GotoISI>://A1986F986900012.

Crutzen, P. J. and M. O. Andreae, 1990: Biomass Burning in the Tropics - Impact on Atmospheric Chemistry and Biogeochemical Cycles. *Science*, **250 (4988)**, 1669–1678, URL <GotoISI>://A1990EN92000032.

Eck, T. F., et al., 2013: A seasonal trend of single scattering albedo in southern African biomass-burning particles: Implications for satellite products and estimates of emissions for the world's largest biomass-burning source. *JOURNAL OF GEOPHYSICAL RESEARCH-ATMOSPHERES*, **118 (12)**, 6414–6432, doi:{10.1002/jgrd.50500}.

Forster, P. and V. Ramaswamy, 2007: Changes in Atmospheric Constituents and in Radiative Forcing. *Climate Change 2007: The Physical Science Basis*, 129–234, URL <GotoISI>://000292238900004.

Frisch, A. S., C. W. Fairall, and J. B. Snider, 1995: Measurement of Stratus Cloud and Drizzle Parameters in Astex with a K-Alpha-Band Doppler Radar and a Microwave Radiometer. *Journal of the Atmospheric Sciences*, **52 (16)**, 2788–2799, URL <GotoISI>://A1995RN65500008.

Haywood, J., S. Osborne, and S. Abel, 2004: The effect of overlying absorbing aerosol layers on remote sensing retrievals of cloud effective radius and cloud optical depth. *QUARTERLY JOURNAL OF THE ROYAL METEOROLOGICAL SOCIETY*, **130 (598, A)**, 779–800, doi:{10.1256/qj.03.100}.

Ignatov, A., et al., 2005: Two MODIS aerosol products over ocean on the Terra and Aqua CERES SSF datasets. *JOURNAL OF THE ATMOSPHERIC SCIENCES*, **62 (4)**, 1008–1031, doi:{10.1175/JAS3383.1}.

Jacobson, M. Z., Y. J. Kaufman, and Y. Rudich, 2007: Examining feedbacks of aerosols to urban climate with a model that treats 3-D clouds with aerosol inclusions. *Journal of Geophysical Research-Atmospheres*, **112 (D24)**, doi: ArtnD24205Doi10.1029/2007jd008922, URL <GotoISI>://000252013700013.

Jiang, H. L., G. Feingold, and W. R. Cotton, 2002: Simulations of aerosol-cloud-dynamical feedbacks resulting from entrainment of aerosol into the marine boundary layer during the Atlantic Stratocumulus Transition Experiment. *Journal of Geophysical Research-Atmospheres*, **107 (D24)**, doi:Artn4813Doi10.1029/2001jd001502, URL <GotoISI>://000181262000008.

Jonas, P., 1996: Turbulence and cloud microphysics. *ATMOSPHERIC RESEARCH*, **40 (2-4)**, 283–306, doi:{10.1016/0169-8095(95)00035-6}.

Kacenelenbogen, M., et al., 2014: An evaluation of caliop/calipso's aerosol-above-cloud detection and retrieval capability over north america. *Journal of Geophysical Research: Atmospheres*, **119 (1)**, 230–244, doi:10.1002/2013JD020178, URL http://dx.doi.org/10.1002/2013JD020178.

Kaufman, Y. J., I. Koren, L. A. Remer, D. Rosenfeld, and Y. Rudich, 2005: The effect of smoke, dust, and pollution aerosol on shallow cloud development over the Atlantic Ocean. *Proceedings of the National Academy of Sciences of the United States of America*, **102 (32)**, 11 207–11 212, doi:Doi10.1073/Pnas.0505191102, URL <GotoISI>://000231253400017.

Kim, M.-H., S.-W. Kim, S.-C. Yoon, and A. H. Omar, 2013: Comparison of aerosol optical depth between caliop and modis-aqua for caliop aerosol subtypes over the ocean. *Journal of Geophysical Research: Atmospheres*, **118 (23)**, 13,241–13,252, doi:10.1002/2013JD019527, URL `http://dx.doi.org/10.1002/2013JD019527`.

Koren, I., L. A. Remer, Y. J. Kaufman, Y. Rudich, and J. V. Martins, 2007: On the twilight zone between clouds and aerosols. *GEOPHYSICAL RESEARCH LETTERS*, **34 (8)**, doi:{10.1029/2007GL029253}.

L'Ecuyer, T. S., W. Berg, J. Haynes, M. Lebsock, and T. Takemura, 2009: Global observations of aerosol impacts on precipitation occurrence in warm maritime clouds. *Journal of Geophysical Research-Atmospheres*, **114**, doi: ArtnD09211Doi10.1029/2008jd011273, URL `<GotoISI>://000265930400005`.

Liu, Y. G., B. Geerts, M. Miller, P. Daum, and R. McGraw, 2008: Threshold radar reflectivity for drizzling clouds. *Geophysical Research Letters*, **35 (3)**, doi:ArtnL03807Doi10.1029/2007gl031201, URL `<GotoISI>://000253063700001http://www.agu.org/journals/gl/gl0803/2007GL031201/2007GL031201.pdf`.

Loeb, N. and N. Manalo-Smith, 2005: Top-of-atmosphere direct radiative effect of aerosols over global oceans from merged CERES and MODIS observations. *JOURNAL OF CLIMATE*, **18 (17)**, 3506–3526, doi:{10.1175/JCLI3504.1}.

Loeb, N. G. and G. L. Schuster, 2008: An observational study of the relationship between cloud, aerosol and meteorology in broken low-level cloud conditions. *JOURNAL OF GEOPHYSICAL RESEARCH-ATMOSPHERES*, **113 (D14)**, doi:{10.1029/2007JD009763}.

Lu, M. L. and J. H. Seinfeld, 2005: Study of the aerosol indirect effect by large-eddy simulation of marine stratocumulus. *Journal of the Atmospheric Sciences*, **62 (11)**, 3909–3932, URL `<GotoISI>://000233460600004`.

Marchand, R., G. G. Mace, T. Ackerman, and G. Stephens, 2008: Hydrometeor Detection Using Cloudsat—An Earth-Orbiting 94-GHz Cloud Radar. *Journal of Atmospheric and Oceanic Technology*, **25**, 519–533, doi:10.1175/2007JTECHA1006.1.

Matheson, M. A., J. A. Coakley, Jr., and W. R. Tahnk, 2006: Multiyear Advanced Very High Resolution Radiometer observations of summertime stratocumulus collocated with aerosols in the northeastern Atlantic. *JOURNAL OF GEOPHYSICAL RESEARCH-ATMOSPHERES*, **111 (D15)**, doi:{10.1029/2005JD006890}.

Nakajima, T. and M. King, 1990: Determination of the optical-thickness and effective particle radius of clouds from reflected solar-radiation measurements .1. theory. *journal of the atmospheric sciences*, **47 (15)**, 1878–1893, doi:{10.1175/1520-0469(1990)047⟨1878:DOTOTA⟩2.0.CO;2}.

Omar, A. H., et al., 2009: The CALIPSO Automated Aerosol Classification and Lidar Ratio Selection Algorithm. *Journal of Atmospheric and Oceanic Technology*, **26 (10)**, 1994–2014, doi:10.1175/2009JTECHA1231.1, URL `http://dx.doi.org/10.1175/2009JTECHA1231.1`.

Painemal, D. and P. Zuidema, 2011: Assessment of MODIS cloud effective radius and optical thickness retrievals over the Southeast Pacific with VOCALS-REx in situ measurements. *Journal of Geophysical Research-Atmospheres*, **116**, doi: ArtnD24206Doi10.1029/2011jd016155, URL `<GotoISI>://000298747600001`.

Pawlowska, H. and J. L. Brenguier, 2003: An observational study of drizzle formation in stratocumulus clouds for general circulation model (GCM) parameterizations. *Journal of Geophysical Research-Atmospheres*, **108 (D15)**, doi: Artn8630Doi10.1029/2002jd002679, URL `<GotoISI>://000184805900007`.

Pawlowska, H., J. L. Brenguier, and L. Schuller, 1999: Microphysical and radiative properties of stratocumulus. *Physics and Chemistry of the Earth Part B-Hydrology Oceans and Atmosphere*, **24 (8)**, 927–932, URL `<GotoISI>://000083562600009`.

Penner, J. E., S. Y. Zhang, and C. C. Chuang, 2003: Soot and smoke aerosol may not warm climate. *Journal of Geophysical Research-Atmospheres*, **108 (D21)**, doi:Artn4657Doi10.1029/2003jd003409, URL

<GotoISI>://000186396400001http://www.agu.org/journals/jd/jd0321/2003JD003409/2003JD003409.pdf.

Petters, J. L., H. Jiang, G. Feingold, D. L. Rossiter, D. Khelif, L. C. Sloan, and P. Y. Chuang, 2013: A comparative study of the response of modeled non-drizzling stratocumulus to meteorological and aerosol perturbations. *ATMOSPHERIC CHEMISTRY AND PHYSICS*, **13 (5)**, 2507–2529, doi:{10.5194/acp-13-2507-2013}.

Powell, K. and M. Vaughan, 2013: Cloud-aerosol lidar infrared pathfinder satellite observations: Data management system-data products catalog. URL http://www-calipso.larc.nasa.gov/products/CALIPSO_DPC_Rev3x6.pdf.

Quaas, J., O. Boucher, N. Bellouin, and S. Kinne, 2008: Satellite-based estimate of the direct and indirect aerosol climate forcing. *JOURNAL OF GEOPHYSICAL RESEARCH-ATMOSPHERES*, **113 (D5)**, doi:{10.1029/2007JD008962}.

Roberts, G., M. J. Wooster, and E. Lagoudakis, 2009: Annual and diurnal african biomass burning temporal dynamics. *Biogeosciences*, **6 (5)**, 849–866, URL <GotoISI>://000266556300009.

Rosenfeld, D., 2000: Suppression of rain and snow by urban and industrial air pollution. *Science*, **287 (5459)**, 1793–1796, URL <GotoISI>://000085775300034http://www.sciencemag.org/content/287/5459/1793.full.pdf.

Rosenfeld, D., H. Wang, and P. J. Rasch, 2012: The roles of cloud drop effective radius and LWP in determining rain properties in marine stratocumulus. *GEOPHYSICAL RESEARCH LETTERS*, **39**, doi:{10.1029/2012GL052028}.

Sekiguchi, M., T. Nakajima, K. Suzuki, K. Kawamoto, A. Higurashi, D. Rosenfeld, I. Sano, and S. Mukai, 2003: A study of the direct and indirect effects of aerosols using global satellite data sets of aerosol and cloud parameters. *JOURNAL OF GEOPHYSICAL RESEARCH-ATMOSPHERES*, **108 (D22)**, doi:{10.1029/2002JD003359}.

Tanre, D., Y. Kaufman, M. Herman, and S. Mattoo, 1997: Remote sensing of aerosol properties over oceans using the MODIS/EOS spectral radiances. *JOURNAL OF GEOPHYSICAL RESEARCH-ATMOSPHERES*, **102 (D14)**, 16 971–16 988, doi:{10.1029/96JD03437}.

Twohy, C. H., J. A. Coakley, Jr., and W. R. Tahnk, 2009: Effect of changes in relative humidity on aerosol scattering near clouds. *JOURNAL OF GEOPHYSICAL RESEARCH-ATMOSPHERES*, **114**, doi:{10.1029/2008JD010991}.

Twomey, S., 1974: Pollution and Planetary Albedo. *Atmospheric Environment*, **8 (12)**, 1251–1256, URL `<GotoISI>://A1974U971800003`.

Twomey, S., 1977: Influence of pollution on shortwave albedo of clouds. *JOURNAL OF THE ATMOSPHERIC SCIENCES*, **34 (7)**, 1149–1152, doi:{10.1175/1520-0469(1977)034⟨1149:TIOPOT⟩2.0.CO;2}.

Twomey, S. and K. Seton, 1980: Inferences of gross microphysical properties of clouds from spectral reflectance measurements. *journal of the atmospheric sciences*, **37 (5)**, 1065–1069, doi:{10.1175/1520-0469(1980)037⟨1065:IOGMPO⟩2.0.CO;2}.

Várnai, T. and A. Marshak, 2009: Modis observations of enhanced clear sky reflectance near clouds. *Geophysical Research Letters*, **36 (6)**, n/a–n/a, doi:10.1029/2008GL037089, URL http://dx.doi.org/10.1029/2008GL037089.

Wang, J. Y. and B. Geerts, 2003: Identifying drizzle within marine stratus with W-band radar reflectivity. *Atmospheric Research*, **69 (1-2)**, 1–27, doi:Doi10.1016/J.Atmosres.2003.08.001, URL <GotoISI>://000187154900001http://ac.els-cdn.com/S0169809503001133/1-s2.0-S0169809503001133-main.pdf?_tid=9d6d1e0e4b5da6b453562e2fbf39d4eb&acdnat=1335282270_5f98e95b4fa848c107a5827d4f70ce17.

Wen, G., A. Marshak, R. F. Cahalan, L. A. Remer, and R. G. Kleidman, 2007: 3-d aerosol-cloud radiative interaction observed in collocated modis and aster images of cumulus cloud fields. *Journal of Geophysical Research: Atmospheres*, **112 (D13)**, n/a–n/a, doi:10.1029/2006JD008267, URL http://dx.doi.org/10.1029/2006JD008267.

Winker, D. M., M. A. Vaughan, A. Omar, Y. Hu, K. A. Powell, Z. Liu, W. H. Hunt, and S. A. Young, 2009: Overview of the CALIPSO Mission and CALIOP

Data Processing Algorithms. *JOURNAL OF ATMOSPHERIC AND OCEANIC TECHNOLOGY*, **26 (11)**, 2310–2323, doi:{10.1175/2009JTECHA1281.1}.

Wu, L., H. Su, and J. H. Jiang, 2013: Regional simulation of aerosol impacts on precipitation during the East Asian summer monsoon. *JOURNAL OF GEOPHYSICAL RESEARCH-ATMOSPHERES*, **118 (12)**, 6454–6467, doi:{10.1002/jgrd.50527}.

Zhang, J., J. S. Reid, and B. N. Holben, 2005: An analysis of potential cloud artifacts in modis over ocean aerosol optical thickness products. *Geophysical Research Letters*, **32 (15)**, n/a–n/a, doi:10.1029/2005GL023254, URL `http://dx.doi.org/10.1029/2005GL023254`.